BIO-ALGORITHMS AND MED-SYSTEMS

Vol. 3, No. 6
2007

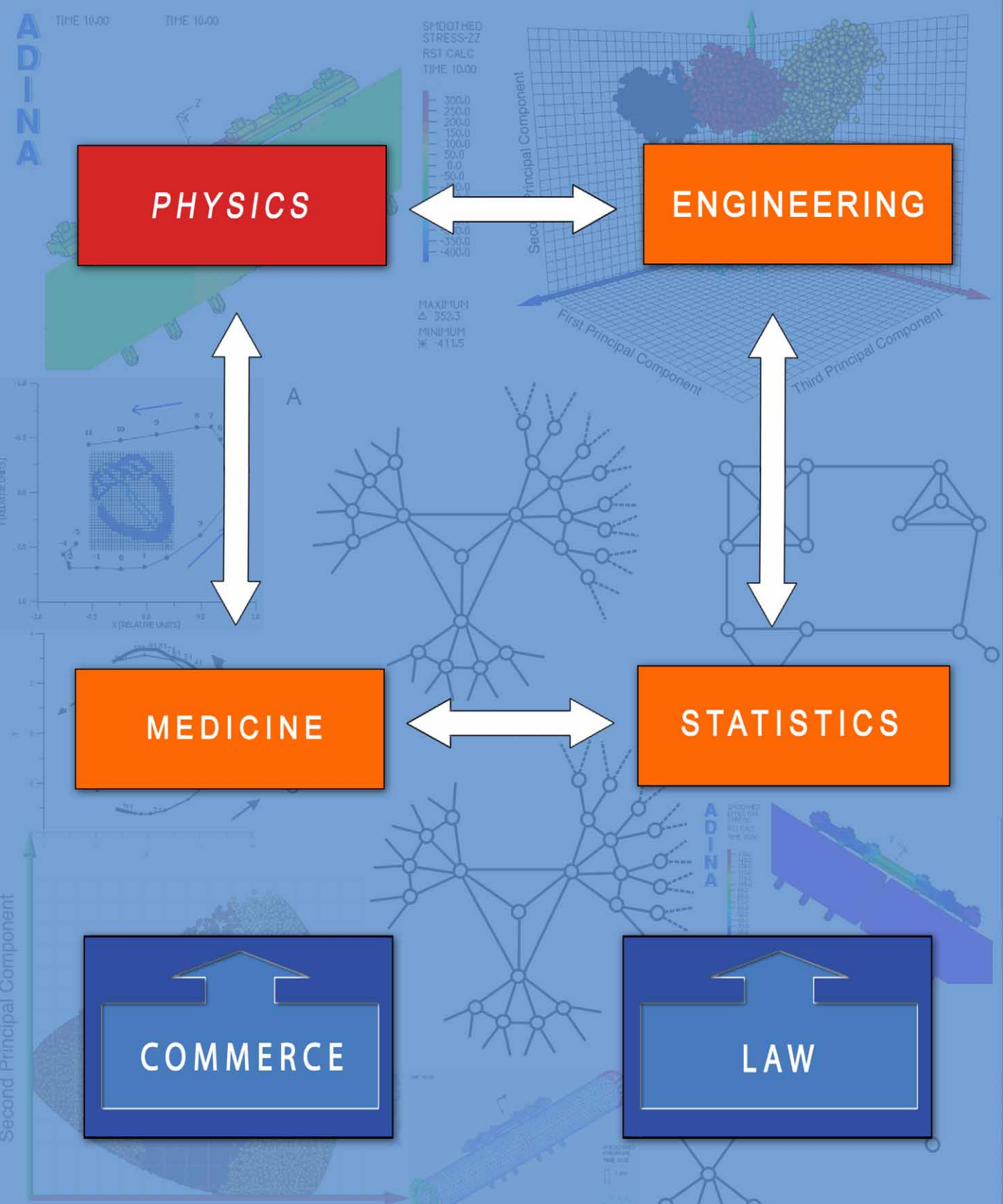

JOURNAL EDITED BY MEDICAL COLLEGE - JAGIELLONIAN UNIVERSITY – KRAKOW – POLAND
http://www.bams.cm-uj.krakow.pl

Contents

BIO-ALGORITHMS AND MED-SYSTEMS
JOURNAL EDITED BY MEDICAL COLLEGE – JAGIELLONIAN UNIVERSITY
Vol. 3, No. 6, 2007, pp. 3-5

INTERNATIONAL SOCIETY FOR TELEMEDICINE AND eHEALTH (ISfTeH)

MIĘDZYNARODOWE TOWARZYSTWO TELEMEDYCYNY I eZDROWIA

ROBERT RUDOWSKI

Department of Medical Informatics and Telemedicine Medical University of Warsaw

Acknowledgment: The author greatfully acknowledge help of Frank Lievens (ISfTeH Board) in preparing this manuscript.

ABSTRACT: The paper presents International Society for Telemedicine and eHealth. In the Introduction the history of the Society, starting from establishing in Kobe, Japan in1997, is described. Next the types of membership are listed. Following the mission, cooperation with key institutions (WHO among them) and activities are described. The mission of the ISfTeH is: *The ISfTeH exists to facilitate the international dissemination of knowledge and experience in Telemedicine and eHealth and to provide access to recognized experts in the field worldwide.* The main ISfTeH activities are: the organization of annual international eHealth/telemedicine conferences, support for local conferences and start-up of national societies. Activities correspond to Working Groups which are Newsletter & Communication, Students and Education. Activity in which the author of the paper has been engaged is the promotion and dissemination of tools for achieving semantic interoperability, namely SNOMED CT. The registration of a new society in Poland – Polish Society of eHealth (PSeH) and the application for ISfTeH membership is mentioned. In Summary the opportunities given by the ISfTeH membership are listed.

Keywords: ISfTeH, mission, cooperation, activities, interoperability, eHealth.

1. INTRODUCTION

HISTORY

Founding of the International Society for Telemedicine (ISfT) took place at the Third International Conference on the Medical Aspects of Telemedicine in Kobe, Japan in May 1997. Founder's Committee included many well known experts in medicine and telemedicine from all continents – DeBakey (USA), Medvedev (Russia), Hjelm (Hong Kong), Rossing (Denmark), Yellowlees (Australia), Lareng (France), Bracale (Italy), McGee (UK), Tanaka (Japan) and many others. At the Seventh International Conference held in Regensburg, Germany in 2002 the decision was made to change the formula of the Society more into a federation of national organizations. The important role played Professor Michael Nerlich, later elected the President of a new Society. The decision was endorsed on September 15th 2003 in Tromsö, Norway at the Eighth International Conference and "ISfT-2" was established as "Not-for-profit" organization under the Swiss law. Founding Members were: Michael Nerlich (Germany), Andre Petitet (France) and Robert Rudowski (Poland).

The Members of the first Board of Directors of the renewed ISfT were:
Frank Lievens (Belgium) – Treasurer,
Jarmo Reponen (Finland),

Robert Rudowski (Poland),
Michael Nerlich (Germany) – President,
Ricky Richardson (UK) – V-ce President,
James O'D McGee (UK),
Lars Hulbaek (Denmark),
Marian Noga (Poland).

The General Assembly of the ISfT held on 6th of April 2005 in Luxemburg voted for a new name of the Society – International Society for Telemedicine and eHealth to be more along the line of such organizations as World Health Organization (WHO), International Telecommunication Union (ITU) and European Union (EU) promoting eHealth name. The logo has been changed to adapt to the new name.

New Board of Directors was elected electronically on Sept. 30th and Oct. 15th 2007 and approved by the General Assembly on December 5th 2007 in Regensburg.

The Members of the new Board who will hold their positions until 2010 are:
Oleg Orlov (Russia), Jarmo Reponen (Finland), Yunkap Kwankam (special invited guest from WHO), Michael Nerlich (Germany), Louis Lareng (France), Trevor Cradduck (Canada), Andre Petitet (France), Frank Lievens (Belgium), Andy Fischer (Switzerland), Moretlo Molefi (South Africa), Steve Normandin (USA), Ricky Richardson (UK).

2. TYPES OF MEMBERSHIP IN THE ISfTeH

There are several types of membership in the ISfTeH:
– national members – national societies of telemedicine and eHealth,
– associate members – other societies of telemedicine and eHealth,
– institutional members – institutions,
– corporate members – commercial firms,
– individual members – if the national society is non existent then a person can join the society as an individual member.

In 2007 the number of members in each category was following:

National	26
Associate	3
Institutional	17
Corporate	9
Individual	37
Students	31

The societies of telemedicine / eHealth from the following countries were ISfTeH national members in 2007: Argentina, Austria, Bangladesh, Bosnia & Herzegovina, Brazil, Canada, Croatia, Denmark, Democratic Republic of Congo, Finland, France, Georgia, Germany, India, Italy, Japan, Kosova, Malaysia, Netherlands, Nigeria, Poland, Russia, Switzerland, Ukraine, UK, Venezuela.

3. MISSION, COOPERATION, ACTIVITIES

The declared mission of the IsfTeH is:
The ISfTeH exists to facilitate the international dissemination of knowledge and experience in Telemedicine and eHealth and to provide access to recognized experts in the field worldwide.

ISFTeH is a non governmental and not-for-profit society. It serves primarily as an umbrella association for national telemedicine & eHealth organizations.

The ISfTeH cooperates with International Telecommunication Union (ITU), World Health Organisation (WHO) and has Alliance Partnership with United Nations Office for Outer Space Affairs (UNOOSA). The great step forward was that in January 2008 WHO Executive Board accepted the International Society for Telemedicine and eHealth as Non Governmental Organization in Official Relation with WHO. The decision underlines the role of the ISfTeH.

The activities of the ISfTeH include:
– promotion and support of telemedicine and eHealth activities worldwide,
– assisting the start-up of new national organizations,
– supporting developing countries in the fields of telemedicine and eHealth.

The IsfTeH is acting as moderator in all aspects of healthcare, feeder of information and projects, coordinator between science, education and implementation, and activator of networking and development.

The ISfTeH International Conferences since 1993 were:

– 1993 Tromsö, Norway
– 1995 Rochester, U.S.A.
– 1997 Kobe, Japan
– 1999 Jerusalem, Israel
– 2000 Montreal, Canada
– 2001 Uppsala, Sweden
– 2002 Regensburg, Germany
– 2003 Tromsö, Norway
– 2004 Brisbane, Australia
– 2005 Sao Paulo, Brazil
– 2006 CapeTown, South Africa
– 2007 Chennai, India.

The conferences supported by the ISfTeH in 2007 were:

– ICDS 2007 – TELEMED 2007 Guadeloupe, French Caribbean (05.01. – 07.01.2007)
– NICTe 2007 – Enugu, Nigeria (07.03. – 09.03.2007)
– 3rd International Conference "Telemedicine – Experience@Prospects" Donetsk, Ukraine (27.03. – 29.03.2007)
– Med-e-Tel 2007 – Luxembourg, Grand Duchy of Luxembourg (18.04 – 20.04.2007)
– Cross-border eHealth in the Baltic Sea Region – Healthcare delivery for the patients of today and tomorrow – Stockholm, Sweden (21.05. – 22.05.2007)
– Telehealth 2007, The Third IASTED International Conference on Telehealth – Montreal, Quebec, Canada (30.05 – 01.06.2007)
– TTeC 07 – Tromsö, Norway (11.06. – 13.06.2007)
– Telemedicine Society of India, 3rd National Conference Chennai, India (2-4.11.2007).

Newsletter & Communication

One of the interesting activities of the IsfTeH is the newsletter activity. Ekaterina Kldiashvili, MD, PhD is the Head of Newsletter and Communication Working Group. The Newsletter was reactivated with Volume 1, Issue 1 released in February 2008. The Newsletter will be issued on a quarterly basis.

The interesting idea which Newsletter Working Group would like to introduce is the creation of international experts's panel for second opinion consultations. The implementation will take place through Forum at ISfTeH website.

The following chapters are listed in Issue 1: Board news, News/contributions from the members, News from partners, Publications, Upcoming events.

The Newsletter is with no doubt a very useful tool for information exchange on telemedicine/eHealth topics.

Activities for students

Recently the establishment of the ISfTeH Student's Working Group has been announced. The Students Working Group is headed by Frank Lievens MSc and two researchers from Brazil : Professor Thais Russomano MD, PhD and Adolfo Sparenberg MD, MSc.

The move is based on the opinion that the worldwide inclusion of students in Telemedicine and e-Health projects is a key component for their success and sustainability.

The ISfTeH announced a new and special activity for the student members: "the ISfTeH Student's Virtual Session".

This is an initiative that aims to promote the active participation of associated students during official ISfTeH Meetings. This new session format will allow the remote presentation of student's projects and researches in eHealth, using Powerpoint or videoconference technologies. The first and exciting opportunity is the upcoming

Med-e-Tel in Luxembourg (16-18 April 2008, www.medetel.lu), where five abstracts will be selected for presentation.

To encourage the world wide participation of students in this new "Virtual Session", the ISfTeH Board decided to offer an award for the best student's presentation.

The proposed awards encourage students to take active part in international telemedicine / eHealth events.

Working Groups , Special Interest Groups (SIG), Closed Interest G roups (CIG)

In addition to already existing Working Groups: Sudents, Newsletter & Communication, Education, the ISfTeH Board proposes a new feature on ISfTeH – Forum in order to enhance international information exchange on telemedicine and eHealth [1].Within this Forum, there are openly available categories and topics for Special Interest Groups (SIGs) and Closed User Groups (CUGs). The latter are only password-accessible. All members interested in participating need to register before they can start their activity. The mere reader or viewer of content, of course, does not need to register.

The moderators will take care of form and content of each section. Members are absolutely free to discuss any pertaining topic.

4. MY PERSONAL ACTIVITIES IN THE ISfTeH

My activities in the ISfTeH Board of Directors during the last 2 years were related to the question of semantic interoperability of eHealth systems which in my opinion is fundamental to further development of the domain.

Semantic interoperability is the ability of two (or more) systems to exchange data on the basis of an agreed vocabulary guaranteeing same interpretation (semantics) of notions for the users of the interoperating systems [2].

It is worth considering a great mobility of the people in the European Union and elswhere (e.g. 1 mln Poles working abroad in the EU countries). The tool for achieving semantic interoperability is Systematized Nomenclature of Medicine Clinical Terminology (SNOMED CT) [3]. Recently SNOMED CT Standard Development Organization (SDO) was established with the Headquarters in Copenhagen. There are 9 countries which are members of SDO. SDO is an open organization and in order to obtain wider SNOMED CT dissemination it is desirable that more and more countries join SNOMED CT SDO. The ISfTeH can play an important role in reaching that aim. Joining the organization gives the country a licence for SNOMED CT usage. The necessary step is of course translation of SNOMED CT into local language. So far it has been done by Germany, Spain and Denmark.

I tried to attract the ISfTeH attention to the problem of SNOMED CT dissemination. WHO is very well aware of SNOMED CT importance for further eHealth development.

In Poland the move to join SNOMED CT SDO is awaiting for the Minister of Health decision. The application was formulated by the Centre for Information Systems in Health Care at the Ministry of Health.

5. BARRIERS TO eHEALTH DEVELOPMENT

There are several barriers to eHealth development.

Among them are the cultural barriers related to local traditions concerning health and health care, political and economical – public vs. private health care system, ethical – remote physician/patient relationship and technological – bandwith and lack of interoperability. The legal barriers are licensing of physicians, approval requirements for providers, privacy, security and regulatory issues. Let me remind you relevant Polish laws.

Article 42 of Polish Law of Medical Profession (Dz.U.Nr 226, poz.1943, 2005)

states:

Physician determines the state of health of a person after previous personal examination. The exceptions are the situations described in separate rules.

Polish Code of Medical Ethics (2.01.2004) states:

Physician can undertake the treatment only after previous patient examination. The exceptions are the situations when the advice can be given only at a distance.

The financial barrier in many countries, among them Poland, is no reimbursement for teleconsultations from the national insurer.

Naturally, the ISfTeH activities are directed towards overcoming those barriers.

6. POLISH SOCIETY OF eHEALTH (PSeH)

The new event related to eHealth development in Poland is the registration of Polish Society of eHealth (PSeH) in Warsaw on 9th of January 2008 in the National Court Register. The location of the new Society is at the Department of Medical Informatics and Telemedicine of the Medical University of Warsaw, SP CSK Hospital, Banacha Street 1A, 02-097 Warsaw, Poland.

The aims of the new Society are:

1. The improvement of the health care system by promoting and supporting eHealth understood as introduction of Information and Communication Technologies (ICT) to health care in cooperation of medical, technological, economical, law and media environments.
2. The promotion of knowledge and achievements in the application area of ICT in health care.
3. The initiation and maintenance of research and education activity in eHealth domain.

The author of this paper was elected the President of the new Society.

PSeH which is open to new members (19 members now) will apply for the ISfTeH membership soon.

7. SUMMARY

In summary the opportunities given by the IsfTeH membership can be given:

- Networking within the international Telemedicine/eHealth community
- Exploring and highlighting the existing synergies between the global players
- Set-up support of new national members
- Dissemination of information via the ISfTeH website and newsletters
- Participation in the yearly issue of a Telemedicine Directory
- Access to telemedical networks
- Download of relevant documents
- Participation in Working Groups on telemedical standards and regulations
- Assistance on legal matters
- Organizing and supporting a yearly ISfTeH scientific conference in different continents
- Open dialogue and cooperation with the industry to promote the development and implementation of innovative and practical products & services
- Promotion of the ISfTeH activities via specialized media supporting the existing national members and their activities

REFERENCES

1. ISfTeH Newsletter, February 2008, Vol.1, Issue 1.
2. IsfTeH. http://www.isft.net.
3. R. Rudowski , M. Grabowski, J. Michalik, B. Kaczyński. SNOMED CT standard in eHealth. Is it really needed? Med-e-Tel Proceedings, Luxexpo, Luxemburg 2007, 212-214.

BIO-ALGORITHMS AND MED-SYSTEMS
JOURNAL EDITED BY MEDICAL COLLEGE – JAGIELLONIAN UNIVERSITY
Vol. 3, No. 6, 2007, pp. 11-21

DETECTING CLUSTERS OF MICROCALCIFICATIONS IN HIGH-RESOLUTION MAMMOGRAMS USING SUPPORT VECTOR MACHINES

Marcin Kurdziel[1], Krzysztof Boryczko[1], David A. Yuen[2]

[1] *Institute of Computer Science, AGH University of Science and Technology, al. Mickiewicza 30, 30-059 Kraków, Poland*
{boryczko, kurdziel}@agh.edu.pl
[2] *Minnesota Supercomputing Institute, University of Minnesota Minneapolis, MN 55455, USA*
davey@krissy.geo.umn.edu

Abstract: This paper presents a new method for detecting clusters of microcalcifications in high-resolution digital mammograms. Using cluster analysis, we have designed a descriptive set of mammogram image features which enables precise recognition of microcalcifications. These features are fed into the Support Vector Machine classifier trained to discriminate between normal image occlusions and deposits of calcium in breast tissue. Initial candidates for microcalcifications, i.e. suspicious regions on a mammogram image, are selected by means of a discrete wavelet transform, image filtering and morphological operations. Once microcalcifications are detected, our algorithm assesses whether they form groups (clusters) and for each such group verifies its diagnostic significance. This verification is performed by employing another, appropriately trained, Support Vector Machine classifier. Accuracy of our system has been evaluated on the Breast Cancer Research Program (BCRP) volumes of the DDSM database. On this largest publicly available databases of mammograms our system achieved a sensitivity of 85.1% with average number of 5.0 false positive detections per image. Such an accuracy is competitive with other published results obtained on the same dataset.

Key words: microcalcification detection, clustering, feature selection, Support Vector Machines

Streszczenie: W artykule przedstawiono nową metodę wykrywania skupisk mikrozwapnień na cyfrowych zdjęciach mammograficznych wysokiej rozdzielczości. Zaproponowana metoda korzysta ze zbioru statystycznych cech obszarów zdjęć mammograficznych, zaprojektowanego za pomocą technik analizy skupisk. Tak skonstruowany zbiór cechy umożliwia precyzyjne rozpoznawania mikrozwapnień. Cechy statystyczne obszarów zdjęć mammograficznych są wykorzystywane przez klasyfikator SVM (od ang. *Support Vector Machine*) wyuczony do rozróżniania pomiędzy normalnymi strukturami na zdjęciach, a okluzjami sugerującymi obecność mikrozwapnień. Pierwotna selekcja podejrzanych obszarów na zdjęciach mammograficznych prowadzona jest za pomocą dyskretnej transformaty falkowej, szeregu operacji filtrowania i morfologicznych przekształceń obrazu. Po wykryciu mikrozwapnień, algorytm ustala, czy tworzą one skupiska. Następnie każde wykryte skupisko oceniane jest pod kątem wartości diagnostycznej. Oceny tej dokonuje kolejny klasyfikator SVM. Skuteczność proponowanej metody została oszacowana na podzbiorze *Breast Cancer Research Program* (BCRP) bazy danych DDSM. Na tej największej publicznie dostępnej bazie danych zdjęć mammograficznych zaproponowana metoda wykazuje czułość na poziomie 85.1% przy średniej liczbie 5.0 wskazań fałszywie dodatnich na jedno zdjęcie. Wynik ten jest konkurencyjny w stosunku do innych opublikowanych rezultatów uzyskanych dla tego samego zbioru zdjęć mammograficznych.

Słowa kluczowe: detekcja mikrozwapnień, analiza skupisk, selekcja cech, Support Vector Machines

1. Introduction

Widespread adoption of Computer-Aided Detection (CAD) systems represents one of the most substantial achievements in medical imaging. Nowadays advanced image processing algorithms constitute an essential part of diagnostic tools such as computer tomography, magnetic resonance imaging or positron emission tomography. Yet, it is the mammography where combination of digital imaging with pattern recognition and artificial intelligence algorithms greatly aid the radiologist in a detection process [1]. It has been known for a long time that an advancement of a malignant breast lesion significantly limits the available therapy options. However, it was only after radiologists began to examine routinely breast radiograms of middle-aged and older women, especially with the use of CAD system, that reliable detection of very subtle cancerous lesions become possible.

Small deposits of calcium, i.e. microcalcifications, are troublesome for visual detection on a mammogram image, in spite of being the most important symptoms of in-situ breast carcino-

mas. Not surprisingly, immense efforts have been undertaken to develop algorithms that would selectively and with high sensitivity detect these types of lesions, thereby allowing for faster and more accurate diagnostic decisions [2]. Unfortunately, currently available methods are far from being perfect and in many cases their evaluation was carried out on small databases containing low or mid-resolution mammograms. Such testing sets are not the best option for evaluating detection of very subtle lesions. Furthermore, an issue of inconsistency in decisions made by CAD systems and their relative accuracy has recently drawn attention of the radiologist community [3]. It is now evident, that the selection of test cases may greatly influence the measured performance of a detection system. To overcome these obstacles an initiative have been started at the University of South Florida, aiming at providing a common ground for comparison between different algorithms for breast cancer detection. The resultant Digital Database for Screening Mammography (DDSM) [4] is the largest and most comprehensive publicly available source of mammogram images.

In this paper, we present a novel detection algorithm, designed specifically for recognition of clusters of microcalcifications in high-resolution mammograms, and evaluate its accuracy on the DDSM database. The algorithm is built over a descriptive set of mammogram features designed, by means of cluster analysis, to provide high classification accuracy while economically utilizing available computational resources. For making decisions, we employ the Support Vector Machine (SVM) classifier [5] whereas initial assessment of possible locations of microcalcifications is carried out using discrete wavelet transform and image filtering operations. Reduction of false-positive detection rate is conducted in two steps – first by classifying individual microcalcifications and afterward by verifying diagnostic importance of the detected clusters.

1.1. Background

The spectrum of computational methods applied to digital mammography is wide [6]. Recognition of microcalcifications, as well as discrimination between benign and malignant lesions, has been traditionally carried out by means of supervised learning techniques, in particular Neural Networks [7] and more recently introduced Support Vector Classifier [8]. Other methods from statistical learning theory have also been studied in this context [9,10]. In searching for possible locations of microcalcifications and enhancement of their visibility wavelet transform [11,12,13] and scale-space approaches [14] have proved to be very successful. Significant effort has been made to develop and employ methods for suppressing intensity dependent noise, inevitable in digital mammograms [15,16]. Furthermore, alternative representations for breast tissue were developed that are more robust against varying imaging conditions than normal intensity-based images [17]. Apart from the aforementioned important approaches, whole range of other pattern recognition tools was used in algorithms for processing and analysis of digital mammograms, including: Singular Value Decomposition and Principal Component Analysis [18,19], fuzzy logic [20], fractal modeling [21] and image filtering techniques [22].

Mammogram volumes from the DDSM database have been employed in several studies concerning detection or assessment of microcalcification clusters. In [23] an evaluation of MammoInsight CAD system is reported, for malignant calcification cases selected from five DDSM volumes. In [24] DDSM was used for evaluation of microcalcification segmentation technique that combine fuzzy c-means algorithm and multidimensional wavelet analysis. In sect. 3, we compare effectiveness of our method to the results reported in these two studies. In [25] a genetic algorithm is employed for deciding whether a given region of interest contains a cluster of microcalcifications or is made of a normal breast tissue. Authors report an area under ROC (i.e. *Az* index) for classification of regions of interest (ROIs), selected from the whole mammogram area, equal to $Az = 0.968$. Study reported in [26] focuses on comparison of effectiveness of SVM and multilayer perceptron (MLP) for the same task. MLP achieved an area under ROC equal to $Az = 0.850$ while the performance of SVM was slightly lower, leading to $Az = 0.826$. In [27] ROI classification method combining linear classification rule and decision tree classifier was described. Authors did not focus on either masses or microcalcifications, but included both types of cancer signatures in the class of abnormal ROIs. The reported area under ROC for a set of ROIs extracted from DDSM mammograms was equal to $Az = 0.98$.

DDSM database was also employed in malignancy assessment task, where the goal is to distinguish between malignant and benign cluster of microcalcifications. In [28] a linear discriminant analysis, employing features derived from ROIs and features provided by radiologists, achieved an area under ROC of $Az = 0.69$. In [29] neural network classifier, also employing a combination of image based and human-provided features, archived 90% classification accuracy for microcalcification clusters. A similar study was described in [30]. Authors report a classification accuracy equal to 74%.

2. Materials and methods

2.1. Database of mammograms

According to the DDSM database policy, the *Breast Cancer Research Program Clustered Microcalcification* volumes, i.e.: BCRP_CALC_0 and BCRP_CALC_1, were used for development and evaluation of our system, respectively. Both these datasets contain 200 high-resolution digital mammograms coming from 50 patients diagnosed with malignant disease marked by clustered microcalcifications. In each case Cranio-Caudal and Mediolateral Oblique views of both the right and left breast are provided. The mammograms were digitized at spatial resolution of 43.5 μm per pixel and 12bps gray-level depth, resulting in a dataset with around 10GBytes of total data volume.

2.2. Selection of Regions of Interest

Selection of suspicious regions on a mammogram image, i.e. ROIs, is carried out by using 2D discrete wavelet transform and image filtering operations. The flowchart of the selection algorithm is depicted in Fig. 1 and the pseudo-code is given in Fig. 9 in Appendix A.

The 2D discrete wavelet transform [31,32] decomposes an image into four set of coefficients, i.e. approximate coefficients *A* and three detail coefficients: horizontal *H*, vertical *V* and diagonal *D*. The approximate coefficients form a representation of an original image with half of the original resolution. The detail coefficients preserve fine structures on the image, that are lost when the image is subsampled onto the lower resolution approximation. The transformation can be carried out recursively, yielding low-resolution, coarse representation of the image and a number of detailed coefficients. This scheme can be useful for detecting microcalcification on a mammogram image. Microcalcifications resemble small, bright protrusion distinguishing from the surrounding background. Therefore, one can assume that the 2D discrete wavelet transform of a mammogram image will preserve the microcalcifications in the detail coefficients, while coarse breast structures, like glandular tissue or muscles, will be confined mostly to the approximate coefficients. Thus, by discarding the approximate coefficients one can suppress a great deal of a normal breast background in mammographic image. Indeed, this is the assumption underlying our ROI selection method. In particular, our algorithm performs 4-level 2D discrete wavelet transform followed by image reconstruction with approximate coefficients set to 0 (steps 1 and 2 in Fig. 9). The depth of the wavelet transform was chosen by visual inspection of several subsampled mammograms from the BCRP_CALC_0 volume, where we could identify the stage of decomposition at which microcalcifications are hardly visible.

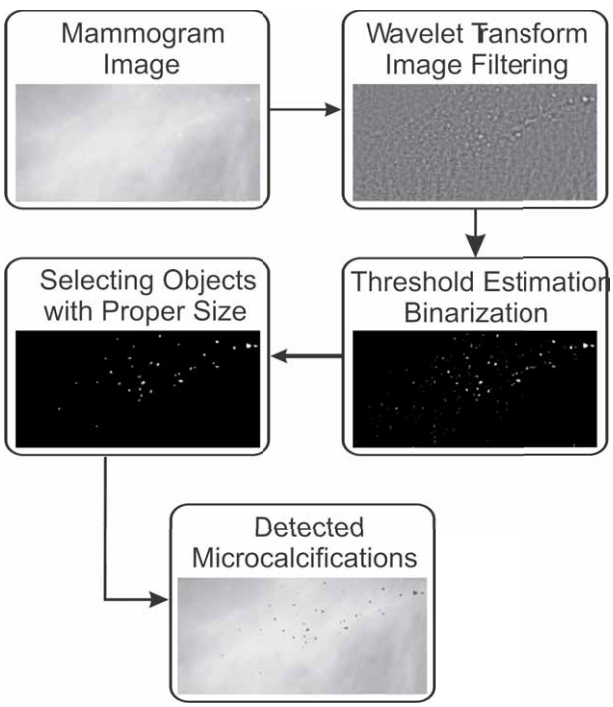

Fig. 1. Flowchart of the algorithm for selecting ROIs on a mammogram image. First, contrast of the mammogram image is enhanced by means of wavelet transform, pixel intensity rescaling and image filtering operations (result depicted in the 2nd block). Next, a threshold value is calculated from the histogram of contrast enhanced image and used to segmentate microcalcification-like objects (3rd block). Afterward, objects whose area or intensity do not correspond to those of microcalcifications are discarded (4th block).

After suppressing mammogram background by wavelet decomposition, we employ image filtering operations to further enhance its contrast and segmentate occlusions suspected of being microcalcifications. First, we address areas of a mammogram image that correspond to radiologically dense breast tissue. To enhance the contrast in these parts of the image, the algorithm linearly scales their pixel intensities. This is done by constructing an enhancing mask (steps 3 and 4 in Fig. 9). The mask do not alter pixels whose intensity is not greater than a threshold value α_1. Pixels with intensity between α_1 and α_2 are scaled by a multiplicative factor ranging from 1.0 to $\beta > 1.0$. The scaling factor is adjusted linearly to the extent by which the pixel intensity exceeds α_1. In areas of saturated image, i.e. where pixel intensity is above α_2 no further increase of scaling factor is done. The threshold values and limit for the scaling factor were adjusted experimentally, by investigating their impact on appearances of microcalcifications in breast regions with radiologically dense tissue. The values were set to $\alpha_1 = 0.75$, $\alpha_2 = 0.9$ and $\beta_1 = 2.5$ (note, that at this step pixel intensities range from 0.0 to 1.0). The image with the dense regions enhanced is denoted by I_r. To be consistent with intensity representation used so far, I_r is linearly rescalled to <0,1> interval.

Further contrast enhancement aims at removal of any normal breast structures, larger than microcalcifications, that could still be present in the image (steps 5 and 6). This is attained by calculating an image I_f consisting of a moving average of the image I_r. The averaging filter of size 20 x 20 pixels is used for this purpose. This filter calculates an average intensity within a sliding rectangular window, 20 x 20 pixels in size, and assigns the average value to the central pixel of the window. The image I_f is substracted from I_r, suppressing the remaining normal breast structures. The size of the averaging filter was chosen to be large enough to dilute microcalcifications during calculation of I_f. Therefore, microcalcifications are not impaired when I_f is substracted from I_r. The image steaming from this step is denoted by I_d and, as it was the case for mask–based enhancing, its intensities are linearly rescalled to <0,1> interval.

In steps 7-10 the algorithm calculates the threshold value used for segmentation of microcalcifications. Instead of fixing the threshold to some constant value, we decided to employ an automatic threshold adjustment scheme. The threshold is estimated from a histogram of pixel intensities in the contrast enhanced image, i.e. I_d. Let the histogram of I_d be denoted by *H*. Typical high resolution mammogram consist of more than ten millions of pixels. Therefore, we employ rather wide histogram, i.e. 5000 bins. The most frequent intensity level in *H* corresponds to the intensity of the background. This is because discrete wavelet transform and average filtering were employed to remove most of the tissue structures from the mammogram. Consequently, the resultant image is to a large extent uniform, with the microcalcifications outnumbered by the background pixels. To mitigate the part of the histogram corresponding to the background, we remove from *H* nine bins centered around the bin with the highest number of assigned pixels (step 8). After adjusting the histogram, the algorithm calculates the threshold value *t* (steps 9 and 10). First, algorithm identifies the new peak of the mammogram, which corresponds to most frequent non–background pixel intensity. The variation of pixel intensities around the peak value, σ, is assumed to be the width of the histogram at the 1/7th of the peak height (see Fig. 2). The threshold value *t* is set to be the weighted mean

of positions of bins in H, increased by σ (Fig. 2). That is, we assume that intensities of microcalcifications exceed the most frequent non–background pixel intensity by σ. This approach aims at removal of low–intensity, small occlusions that are present in high–resolution mammograms, e.g. image noise. The definition of σ was chosen by pinpointing the value, for which any further increase would lead to loss of lowest-intensity microcalcifications.

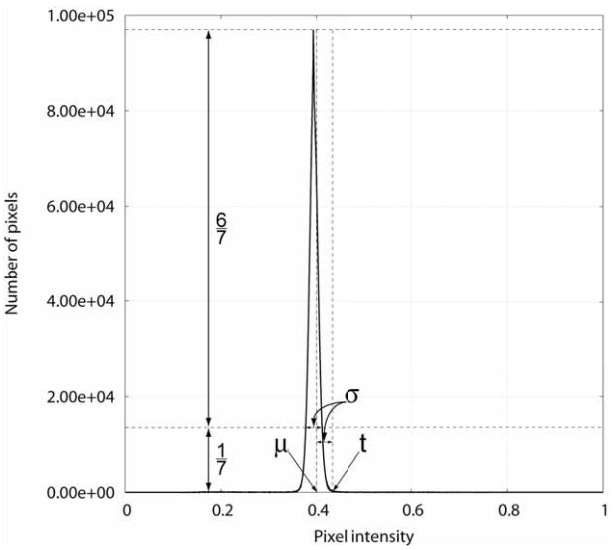

Fig. 2. The method for estimating the threshold value for segmentating microcalcifications.
μ – weighted mean of bins' positions in histogram of contrast enhanced mammogram image, σ – width of the histogram at 1/7th of its height, t – threshold value. The detailed description of the method for calculating the threshold value is given in the Sect. 2.2

After calculating the threshold value t, the algorithm constructs a mask M by thresholding the image I_d. Then, connected components in M, denoted by C_i, are identified (step 11). The connected components represent structures preserved in the binary mask M. These structures are microcalcifications, macrocalcifications, some of the mammogram artifacts and noise that could not be removed by thresholding. To purify M, we focus on the typical size of microcalcifications visible on mammograms (step 12). In particular, objects with an area lower than 6 pixels are removed from M as they resemble salt-like noise, lacking any features that could be used for discriminating them from spurious detections. Object with an area higher than 200 pixels are also removed from M as they represent either macroscopic calcifications or larger image artifacts. Final purification is attained by inspecting geometrical centers of objects still remaining in M. Objects with low pixel intensity at their centers of gravity are discarded (steps 13 and 14). Here, the algorithm employs a conservative threshold of 20% of maximal pixel intensity.

An example result of segmentating microcalcifications using the described technique is presented in Fig. 3. We should note here, that the algorithm was tuned to achieve a high sensitivity to microcalcifications. As the false-positive detections (further called FPs) are discarded by our system in the subsequent steps, by the SVM classifiers, the high specificity was not a primary concern. To evaluate the segmentation method, we have performed a manual inspection of 75 mammogram image regions, chosen from these of the BCRP_CALC_0 images that were not used for estimating the algorithm parameters. Selected regions contained 489 microcalcifications and the segmentation algorithm managed to identify 451 of them, i.e. 92.3%. Remaining 38 microcalcifications, i.e. 7.7%, were missed. Focusing on clusters of microclacifications, the algorithm identified at least two microcalcifications in 98.0% of probable clusters, i.e. in 100 out of 102. The criterion of identifying at least twomicrocalcifications in a given cluster steams from the definition of a suspicious cluster of calcifications, that we adopt in this work. In particular if at least two microcalcifications are identified in close proximity, further steps of the presented system will evaluate them with respect to possible sign of a cancerous process. The number of FPs microcalcifications prompted in the test regions was equal to 467, i.e. 0.96 FPs per probable microcalcification. Similarly, 59 FPs clusters of microcalcification were detected, i.e. 0.58 FPs per probable cluster.

In order to design a descriptive set of features for mammogram image regions and to train the SVM classifiers a set of ROIs is needed. Such a *working dataset* composed of 93,277 ROIs was extracted, using the above-described method, from the BCRP_CALC_0 volume of the DDSM database.

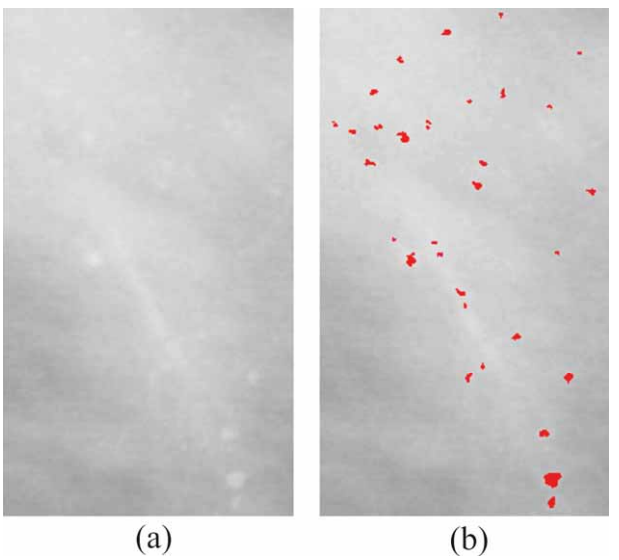

Fig. 3. Result of segmentating microcalcifications in high-resolution mammogram image by using the wavelet algorithm (Fig. 9). (a) Region of a mammogram image containing microcalcifications. (b) The same region, on which we overlaid the result of segmentation.

2.3. Feature extraction from Regions of Interest

The algorithm for selecting ROIs (Sect. 2.2) is sensitive to small objects marked by abrupt changes in pixel intensities. Therefore, it detects not only microcalcifications but also other types of occlusions presented in a mammogram image, including some structures of a normal breast tissue. The removal of these FPs is carried out on the basis of feature vectors containing statistical texture descriptors. Initially, a number of texture descriptors was considered for inclusion in feature

vectors. Their listing is provided in Table 1. The following notation is used:

- R – mammogram region of interest, N x N pixels in size (here, N = 31 for whole ROI and N = 11 when only the central part of the ROI is analyzed),
- H – histogram of the ROI,
- μ_h, σ_h^2 – mean value and variance of the histogram,
- C – second order histogram of the ROI (i.e. co-occurrence matrix) [33]. The matrix C is G x G pixels in size (in this work the size is equal to G = 20).
- μ_{Cx}, μ_{Cy} – mean values of marginal distributions of the histogram C.
- σ_{Cx}, σ_{Cy} – standard deviations of marginal distributions of the histogram C.

The appearance of a microcalcification can vary from a small point at the center of the ROI to an object covering most of the ROI area. To compensate for this variability, we calculated the 23 statistical features from the Table 1 over the whole ROIs area and afterward over their central rectangular part with the size 11 x 11 pixels. Consequently, each ROI was initially described by a 46-dimensional feature vector. However, it should be noted that the features were chosen from commonly used texture characteristics. Therefore, one may expect that some of them are not descriptive in the context of ROI classification. It is also not obvious whether a given feature should be calculated over the whole ROI area, over its central rectangular part or both. To compensate for this, a feature selection scheme was employed and only a selected subset of features was used in subsequent steps.

2.4. Clustering for reducing the dimensionality

Number of ROIs in the *working dataset*, which reaches over 93,000, prohibits their direct visual inspection. However, analysis of this dataset is needed for the subsequent steps of system design, in particular feature selection and training of the SVM classifier. We have decided to overcome this obstacle by performing cluster analysis [34] of the dataset.

First, we carried out classical clustering using the k-means algorithm [35]. Feature vectors were normalized to unit length. The goal was to partition the dataset into several distinct groups and subsequently identify the features whose distributions differ between the groups. The rationale for this approach is that clusters group together ROIs with similar mammographic structures. ROIs belonging to different clusters corresponds to different structures. If a distribution of some feature is equal in each of the clusters, we can assume that the discriminative ability of that feature is low, as the probability that the feature will assume a given value do not depend on the cluster and in turn on the underlying mammographic structure. Therefore, by examining histograms of a the feature in each of the clusters we can perform an initial feature evaluation.

The result of the k-means clustering is presented in the Fig. 4a. Having the dataset clustered, for each of the 46 evaluated features we have calculated six histograms – i.e. one histogram for each of the clusters. Investigation of these histograms revealed that in 19 cases features exhibited only minor differences between the clusters. These features were considered as not useful for discriminating between different types of mammogram ROIs and consequently were removed from

Table 1. Statistical features of mammogram image ROIs.

Mean intensity of pixels	$\mu = \frac{1}{N^2}\sum_{i,j=1}^{N} R_{ij}$
Variance of pixel intensities	$\sigma^2 = \frac{1}{N^2}\sum_{i,j=1}^{N}\left(R_{ij}-\mu\right)^2$
Range of pixel intensities	$r = \max_{i,j=1}^{N} R_{ij} - \min_{i,j=1}^{N} R_{ij}$
Kurtosis of pixel intensities	$\mu_4 = \frac{1}{N^2\sigma^4}\sum_{i,j=1}^{N}\left(R_{ij}-\mu\right)^4$
Skewness of pixel intensities	$\mu_3 = \frac{1}{N^2\sigma^3}\sum_{i,j=1}^{N}\left(R_{ij}-\mu\right)^3$
Fifth and sixth central moments of pixel intensities	$\mu_5 = \frac{1}{N^2\sigma^5}\sum_{i,j=1}^{N}\left(R_{ij}-\mu\right)^5$ $\mu_6 = \frac{1}{N^2\sigma^6}\sum_{i,j=1}^{N}\left(R_{ij}-\mu\right)^6$
Mean absolute deviation of pixel intensities	$m = \frac{1}{N^2}\sum_{i,j=1}^{N}\left\|R_{ij}-\mu\right\|$
Percentiles of pixel intensities	p_x = value greater than x% of pixel intensities and smaller than (100-x)% of pixel intensities; x=10%, 50%, 90%, 95%
Interquartile of pixel intensities	$iq = p_{75} - p_{25}$
Skewness of a ROI histogram	$\mu_{h3} = \frac{1}{N\sigma_h^3}\sum_{i=1}^{N}\left(H_i-\mu_h\right)^3$
Kurtosis of a ROI histogram	$\mu_{h4} = \frac{1}{N\sigma_h^4}\sum_{i=1}^{N}\left(H_i-\mu_h\right)^4$
Entropy of pixel intensities	$S = -\sum_{i=1}^{N} H_i \cdot \log_2 H_i$
Energy of a ROI histogram	$E = \sum_{i=1}^{N} H_i^2$
Entropy of a ROI second order histogram	$S_C = -\sum_{i,j=1}^{G} C_{ij} \cdot \log_2 C_{ij}$
Energy of a ROI second order histogram	$E_C = \sum_{i,j=1}^{G} C_{ij}^2$
Autocorrelation a ROI second order histogram	$\rho = \sum_{i,j=1}^{G} \frac{(i-\mu_{Cx})(j-\mu_{Cy})C_{ij}}{\sigma_{Cx}\sigma_{Cy}}$
Contrast	$\upsilon = \sum_{i,j=1}^{G}(i-j)^2 C_{ij}$
Inverse difference of a ROI second order histogram	$I = \sum_{i,j=1}^{G} \frac{C_{ij}}{1+(i-j)^2}$
Maximum value of a ROI second order histogram	$M_C = \max_{i,j=1}^{G} C_{ij}$

the dataset. The remaining 27 features were included in further evaluation. Fig. 5a presents histograms of an example feature removed from the dataset. Histograms of an example feature showing significant variability between the clusters, and therefore selected for further evaluation, are shown in Fig. 5b.

For further evaluation of features and selection of training examples for the SVM algorithm we have performed clustering of the *working dataset*, narrowed to the 27 features selected previously, with a density-based clustering algorithm [36]. The algorithm was employed to discover compact, dense clusters that correlate with frequent types of ROIs presented in the *working dataset*. A total of 6 clusters were unveiled and are presented in Fig. 4b. With the dataset partitioned, center of gravity C_i was calculated for each cluster. Afterward, following score value was assigned to each feature:

$$S_n = \sum_{i,j=1..6} \sqrt{\sum_{k=0}^{27} \left[C_i(k) - C_j(k)\right]^2} - \sum_{i,j=1..6} \sqrt{\sum_{k=0}^{27} \left[C_i^{(n)}(k) - C_j^{(n)}(k)\right]^2}$$

where $C_i^{(n)}$ denotes the center of gravity of the *i*-th cluster when the *n*-th feature is set to 0. As we can see, the score value S_n reflects the contribution of the *n*-th feature to the sum of distances between the clusters. As such, it measures usefulness of a given feature for discriminating between different types of ROIs. Experimental results revealed, that feature vectors composed of 17 features with the biggest score values enable classification accuracy very close to the accuracy given by all the 46 features initially considered for inclusion into the system (see Sec. 2.5). These 17 features are:

1. *calculated from the central rectangular part of ROI,* 11 x 11 *pixels in size*: 95-th percentile of pixel intensities, entropy of pixel intensities, energy of a histogram, entropy of a second order histogram, inverse difference of a second order histogram.
2. *calculated from the whole area of ROI*: mean intensity of pixels, skewness of pixel intensities, 10th, 50th, 90th and 95th-percentile of pixel intensities, skewness of a histogram, kurtosis of a histogram, entropy of pixel intensities, energy of a histogram, contrast, inverse difference of a second order histogram.

2.5. Classification of Regions of Interest

For training of the SVM classifier, used in recognition of ROIs that contain microcalcifications, we selected a subset of 16,570 examples from the *working dataset*. It was decided, to steer the selection of examples by the cluster memberships obtained previously (see Sect. 2.4). In particular, proportionally larger number of examples was selected from the cluster containing ROIs with microcalcification-like appearances and from the cluster containing ROIs with elongated tissue structures or visible artifacts. The latter ones have been chosen as they were found to be an important source of FPs at the ROI selection step. Visual investigation of the training set revealed 5,890 positive examples and 10,680 negative examples.

Before training of the classifier all the dimensions of feature vectors were normalized to zero mean and unit variance. The estimates of mean values and variances were calculated on the whole *working dataset*. Having the dimensions normalized, each feature vector was also normalized to unit length. For discriminating feature vectors representing microcalcifications from FPs we employed the SVM classifier with a radial basis function (RBF) kernel:

$$k(\mathbf{x}_1, \mathbf{x}_2) = \mathrm{e}^{-\sigma \|\mathbf{x}_1 - \mathbf{x}_2\|^2}.$$

A simulated annealing (SA) scheme was used to establish reasonable values for the SVM misclassification penalty and width of the RBF kernel. Average area under the ROC curve in a 5-fold cross-validation was used as an objective function. The best parameters found by SA were: misclassification penalty equal to C = 28.3 and width of the RBF kernel equal to σ = 0.59. With these parameters the classifier yielded *Az* index

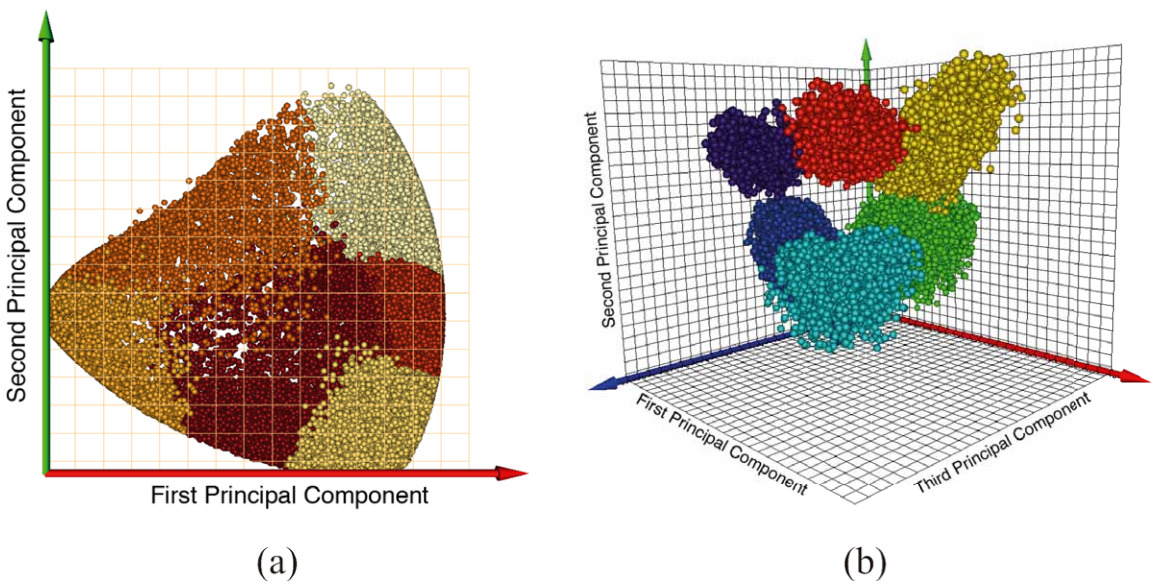

Fig. 4. The result of clustering of the *working dataset* with the k-means algorithm (a) and the density clustering technique (b). The projections from the original, multidimensional space to 2D and 3D spaces were done using the Principal Component Analysis technique.

Brak Fig. 5

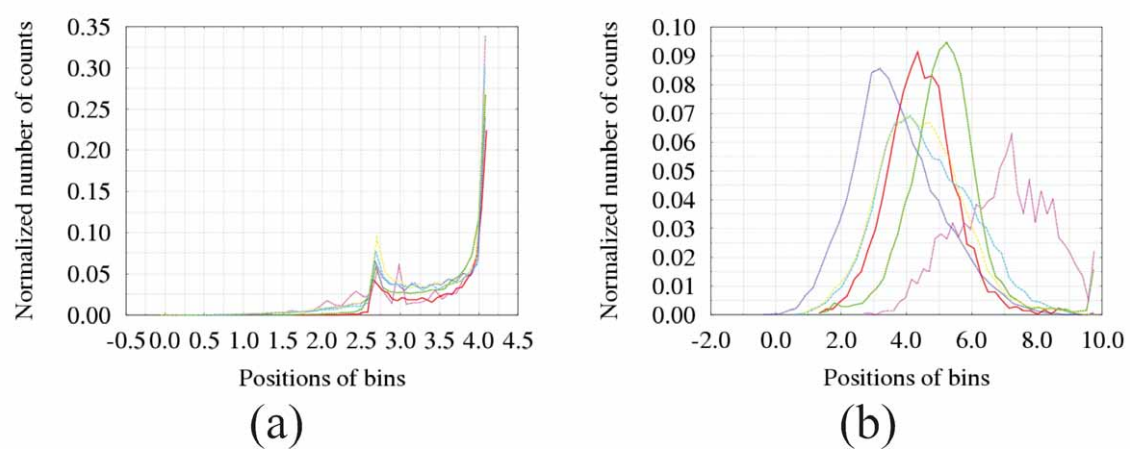

Fig. 5. Histograms of two example ROI features from Table 1. Histograms were calculated separately for each of the clusters found by the k-means algorithm. Values of the feature from diagram (a) are similar in each of the clusters, which makes the feature useless for classification of mammogram ROIs. Values of the feature from diagram (b) differs signifycantly between the clusters.

in a 5-fold cross-validation equal to *Az* = 0.972. Using the corresponding ROC curve a threshold value was adopted for the classifier that yields 92% sensitivity and 92.9% specificity to microcalcifications.

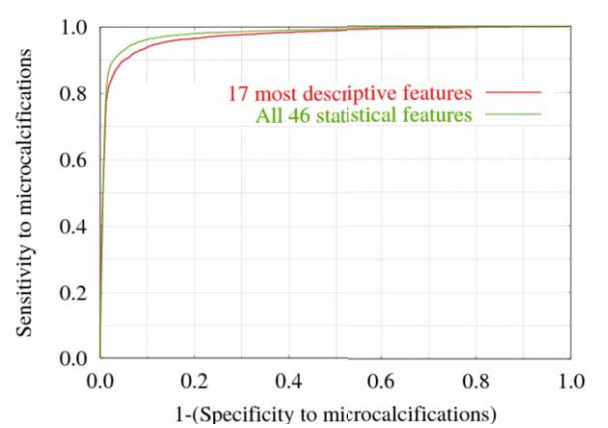

Fig. 6. ROC curves for the SVM classifier used in recognition of ROIs containing microcalcifications. When trained with all available 46 statistical features, the classifier yielded Az index equal to Az = 0.980. The Az index for the classifier trained using the 17 most descriptive features, is equal to Az = 0.972.

In order to investigate the impact of the feature selection step on the accuracy of our system, we have trained another SVM classifier using all the 46 statistical features given in Sect. 2.3. Training and parameter study were performed in exactly the same way as described above. The classifier yielded the *Az* index in a 5-fold cross-validation equal to *Az* = 0.890, which is almost equal to the result obtained when only the 17 most descriptive features are used. The ROC curves for both classifiers are depicted in Fig. 6.

2.6. Detection of microcalcification clusters

Several definitions of a microcalcification cluster can be found in the literature, varying from 3 calcifications in an area of 1.0 cm^2 to 5 calcifications in the volume of 1.0 cm^3 [7, 37]. In this work, we consider a group of at least two calcifications within a radius of 0.5 cm to be a potential origin of a cluster. For reducing the ratio of FPs, each such group is examined by using an SVM classifier trained to recognize suspicious clusters. Once its diagnostic importance is verified, we then add the surrounding microcalcifications to it provided that they are not further than 0.75 cm from the nearest microcalcification already in the group. This procedure is repeated, until no more microcalcifications can be added to the constructed cluster.

Table 2. Features used for classification of clusters of microcalcifications.

Features of the whole cluster	Number of microcalcifications, Mean value and standard deviation of distances between centers of gravity of microcalcifications, p-value for correlation coefficient between coordinates of microcalcifications gravity centers
Features of microcalcifications	Mean value, standard deviations, minimal and maximal value of: microcalcification area, length of microcalcification perimeter divided by its area, ratio of microcalcification convex hull area to microcalcification area, ratio of microcalcification minor axis length to the major axis length
Texture descriptors	Mean value and standard deviation of pixel intensities, skewness, kurtosis and entropy of a histogram of pixel intensities, entropy and inverse difference of a second order histogram of pixel intensities, contrast (mathematical equations for these features are provided in Table 1)
Other features	Mean value and standard deviation of decision values given by the SVM classifier used for verification of ROIs constituting the cluster

Classification of microcalcification clusters is usually performed with features describing shapes of calcifications and their distribution in the cluster [38,39,40]. We employ for this purpose 30-dimensional feature vectors, in which such geometrical and morphological descriptors are accompanied by features of the cluster texture and information on the decision values given by the SVM classifier used at the ROIs selection step. The detailed listing of the features is given in Table 2. To construct the training set, all possible clusters of microcalcifications were detected in the BCRP_CALC_0 volume of the DDSM database. In total 5702 clusters were identified. Visual investigation of this detections revealed 294 clusters containing calcifications and 4789 FPs. The remaining 619 cases were inconclusive and thus were discarded from the training set. In the course of training, we have used the same kernel function, normalization proceduresand methodology of parameter study as previously employed for ROIs classification (Sect. 2.5). The best results were achieved with the value of misclassification penalty equal to $C = 2.27$ and width of the RBF kernel equal to $\sigma = 0.19$. The classifier yielded the Az index in a 5-fold cross-validation equal to $Az = 0.963$. The ROC curve is presented in the Fig. 7.

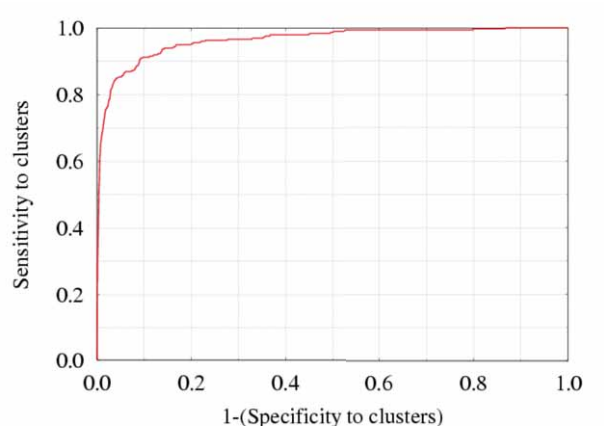

Fig. 7. ROC curve for the SVM classifiers used in recognition of suspicious clusters of microcalcifications. The Az index is equal to $Az = 0.963$.

3. Results

We have evaluated the presented system on the BCRP_CALC_1 volume of the DDSM database. All algorithms were implemented and parameters set, as described in the previous sections. Normalization of features was carried out using estimates of mean value and standard deviation calculated on the BCRP_CALC_0 volume. Several tests have been performed, using different values for thresholding the response of the classifier used in recognition of suspicious clusters. In each test we measured the sensitivity and number of FPs, accordingly to the ground truth marked by radiologists. In few cases detections were observed on the artifacts located outside of the breast region, e.g. embedded date of study. These detections should not focus the attention of radiologists and thus we do not included them in the evaluation. The results, in the form of FROC curves [41], are presented in the Fig. 8. We have provided the collective FROC curve for the whole BCRP_CALC_1 volume, as well as separate FROC curves for microcalcification clusters with different subtlety, which was specified by the radiologist.

The FROC analysis was chosen because the system works as a prompting method, that marks suspicious regions before radiologist inspect the mammogram. Fully automatic mammogram analysis is still beyond capability of computerized detection systems. In particular, false positive detections are frequent in full field mammogram analysis, leading to poor specificity. Best results report a specificity comparable to 0.5 FPs per mammogram image [42]. Still, for prompting method, where the goal is to mark possible locations of microcalcifications for manual inspection by radiologist, such FPs rate can be acceptable.

The highest sensitivity of the proposed method on the DDSM database is equal to 91.1%. However this result can be achieved only at a cost of high number of FPs. In practice, sensitivity should be assumed to be 85.1% at the cost of 5.0 FPs per image, 83.2% at the cost of 4.0 FPs per image and 79.2% at the cost of 2.8 FPs per image. From Fig. 8b we can see that the sensitivity varies significantly depending on the subtlety of the clusters. In particular, up to 100% of clusters of subtlety 4 can be detected with the average number of FPs less than

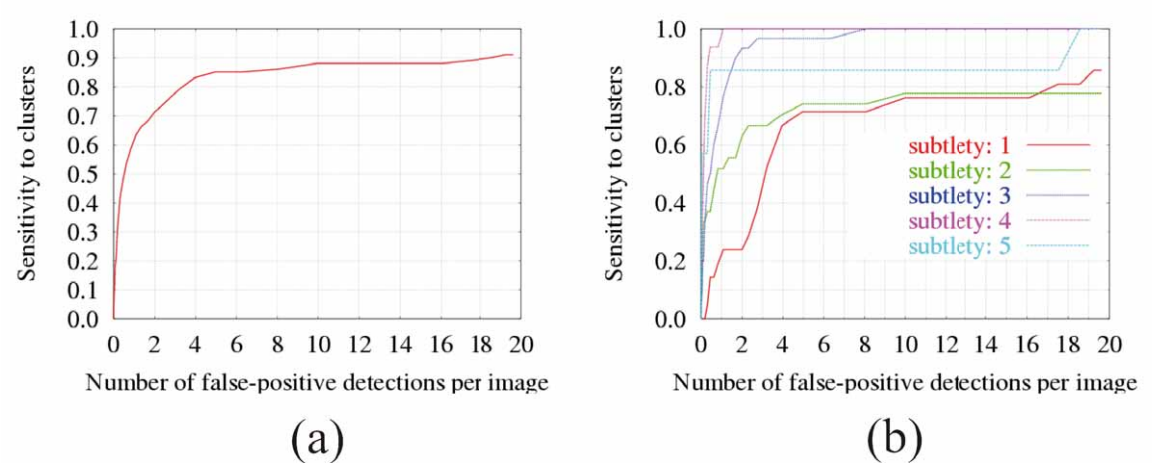

Fig. 8. Free-response Receiver Operating Characteristics (FROC curves) of the proposed system for detecting clusters of microcalcifications. The results were obtained on the BCRP_CALC_1 volume of the DDSM database. (a) FROC curve for the whole BCRP_CALC_1 volume. (b) FROC curves for microcalcification clusters of different subtlety, as specified by the radiologists

1.1 per image. Similarly, 90% of clusters of subtlety 3 can be detected at the cost of 1.7 FPs per image. The result for the microcalcification clusters of subtlety 5 should be taken with caution. The BCRP_CALC_1 volume contains only 7 clusters of this type, 6 of which were detected at the average number of 0.46 FPs per image. Detection of very subtle clusters (i.e. subtlety of 1 or 2) is more troublesome. In particular, it is possible to detect 71.4% of clusters of subtlety 1 and 74.1% of clusters of subtlety 2 while keeping the FPs at the rate of 5.0 per image.

One should note, that the highest sensitivity to clusters of subtlety 1 is greater than the highest sensitivity to clusters of subtlety 2 (85.7% vs. 77.8%). The analysis of mammograms in which the algorithm failed to recognize suspicious lesion revealed, that in 66.6% of cases the clusters consisted of either punctate or amorphous microcalcifications (as marked by the radiologist). Microcalcifications of these types occur in 40% of lesions with subtlety 2 and in 33% of lesions with subtlety 1. This suggests that amorphous and punctate microcalcifications are the most difficult to recognize using the proposed method.

The bests results reported in the literature reach sensitivity of 90% with average number of 0.5 FPs per mammogram image [42]. However, for the DDSM database [43] reports sensitivity of the method presented in [42] to be 70% with average number of 4.0 FPs per mammogram image. At the sensitivity level of 70% the algorithm presented in this article generates 2.0 FPs per mammogram, which is a result competitive to the one given in [43]. DDSM database was also employed in [23] and [24]. These studies did not use BCRP calcification volumes, instead relaying on a manual selection of microcalcification cases. Fortunately, in both cases Authors report distribution of microcalcification cluster subtleties, which greatly simplifies comparison to our method. The distributions of cluster subtleties in the two aforementioned studies and the BCRP_CALC_1 volume, used in our study, are summarized in Table 3. In [23] 86% sensitivity to clusters is reported at the cost of 1.0 FP per image and 90% sensitivity at the cost of 2.0 FPs per image. Yet, comparing to BCRP_CALC_1, the study underrepresents clusters of subtlety 1, which account for 3% of cases (21% in case of BCRP_CALC_1), and overrepresents clusters of subtlety 4 and 5, which account for 20% and 28% of cases respectively (comparing to respectively 16% and 7% of cases in BCRP_CALC_1). Therefore, this dataset is significantly easier than the BCRP_CALC_1 volume. While the microcalcifications of subtlety 1 or 2 are a challenge for our method, those of higher subtlety can be identified much more easily, and at the cost of 1.7 FPs per image we were able to detect six out of seven clusters of subtlety 5, all clusters of subtlety 4 and 90% clusters of subtlety 3. In [24] a sensitivity of 75% is reported at the cost of 3.0 FPs per image and sensitivity of approximately 80% at the cost of 5.0 FPs per image. The reported effectiveness is lower than the results of our method. Comparing to BCRP_CALC_1, the dataset used in this study underrepresents clusters of subtlety 1, which account for 12% of cases and overrepresents clusters of subtlety 2 (41% of cases), 4 (23% of cases) and 5 (23% of cases). Clusters of subtlety 3 were not present in this study. Overpresentation of subtlety 2 clusters should compensate to some extent for the overrepresentation of easy cases (subtlety 4 or 5) and underrepresentation of hardest cases (subtlety 1). Therefore, this volume appears to be overall more balanced than the case selection used in [23].

Table. 3. Distribution of subtleties of microcalcification clusters in the compared studies.

Subtlety	1	2	3	4	5
(Drexi et al., 2003)	5	24	56	34	46
(Sentelle et al., 2002)	2	7	0	4	4
Our work (BCRP_CALC_1)	21	27	28	16	7

4. Concluding remarks

Screening mammography substantially improved diagnosis, and consequently treatment, of the breast cancer. In spite of ever-increasing number of cases diagnosed annually, the death rate is declining [44]. This promising trend may be further accelerated by more reliable cancer detection, stemming from the use of CAD systems [45]. We have presented here our results in developing new CAD algorithms for detecting breast cancers manifested by malignant clusters of microcalcifications. Our method has several advantages over classical approaches to this problem. First, we have employed a density–based clustering algorithm to create efficient classification scheme for recognition of individual microcalcifications. In particular, by means of cluster analysis we have designed small, yet descriptive set of mammogram features, that allow for robust classification of ROIs. Furthermore, we have used the clustering technique to facilitate the selection of large, encompassing set of training examples. Another important aspect of our approach, is the focus on mammograms digitized at high spatial resolution i.e. 43.5 μm per pixel. One should bear in mind that reliable detection of marginally visible lesions depends heavily on the resolution of mammograms. In particular, results presented in [46] suggest that spatial resolution as high as 35 μm might be required for detection of the most subtle microcalcifications. Although mammograms digitized at this resolution are currently not available publicly, the resolution used in our system is still higher than typically used 100.0 μm per pixel [47,48,14,49]. Last but not least, we use two-stage procedure for reducing the rate of FPs, that employs the SVM classification algorithm [5]. This recently developed classifier is well known for its excellent generalization performance [50,51,34].

Evaluation of our method unveiled that at normal operating conditions one should expect an average number of 2 to 5 FPs per mammogram image, depending on the requested sensitivity level. However, we should note here that the BCRP_CALC_1 volume, used in the evaluation, provides the ground-truth marks only for the pathology-proved malignant lesions. Non-malignant clusters presented on the mammogram, if any, are not marked, and in this work their detection is considered as false-positive. In typical screening mammography scenario, the pathology results are not available until suspicious-looking cluster is found and biopsy is performed. Thus, in this context the aforementioned ratio of FPs might be slightly overestimated.

Our future work will focus on two aspects of the proposed approach. First, we will work on improving the accuracy of our system, particularly by increasing the specificity to individual

microcalcifications as well as suspicious clusters. We will also introduce a method for assessing the malignancy probability of detected clusters. This assessment can be carried out using the SVM classifier and a modified version of the currently used set of cluster features. However, the database of example mammograms, used for system training and validation, will have to be extended to incorporate cases with benign lesions. Finally, we should note that in the current design our system does not perform explicit noise equalization. However, it has been shown that noise-equalizing algorithms can improve the overall performance of CAD systems [15,47]. Therefore, we plan to increase the specificity of our method by incorporating this additional technique. We anticipate that it may also lead to increased sensitivity.

Acknowledgements

This research was supported by Digital Technology Center of University of Minnesota, National Science Foundation CMG and ITR programs and Polish Ministry of Science and Higher Education (MNiSW) grants no. 3T11F01030 and 3T11F01930. The authors are also grateful to Prof. Witold Dzwinel and Dr. Tomasz Arodź for their helpful and valuable comments.

A. Appendix. The algorithm for selecting Regions of Interest

INPUT: mammogram image I, $n \times m$ pixels in size. Black color is encoded by 0 whereas white by 1
OUTPUT: a set of rectangular ROIs with size 31×31 pixels each
1. Perform the 4-level 2D discrete wavelet transform of I using spline bi-orthogonal wavelets of order 2
2. I_r = perform image reconstruction with approximate coefficients set to 0

$$\textbf{3. } I_m(k,l) = \begin{cases} 0 & I_r(k,l) < 0.75 \\ 10.0 \cdot (I_r(k,l) - 0.75) + 1 & 0.75 \le I_r(k,l) \le 0.9 \\ 2.5 & I_r(k,l) > 0.9 \end{cases}$$

4. $I_r = I_r \cdot I_m$; Rescale I_r to $\langle 0,1 \rangle$ interval
5. I_f = filter I_r with a 20×20 averaging filter;
6. $I_d = I_r - I_f$; Rescale I_d to $\langle 0,1 \rangle$ interval
7. Compute histogram H of I_d; Store bin values in H_v and bin positions in H_p
8. Remove from H interval consisting of 9 bins centered around the bin with the highest number of assigned pixels
9. H'_p = find positions of bins whose value is below $\frac{1}{7}$ of maximal histogram value
10. $t = \frac{\sum_k H_p(k) \cdot H_v(k)}{\sum_k H_v(k)} + \left[H_p\left(\max_l H'_p(l)\right) - H_p\left(\min_l H'_p(l)\right) \right]$
11. M = segmentate I_d with a threshold value t and find connected components in the resultant image
12. Remove from M components whose area is above 200 pixels or below 6 pixel
13. $\forall c_i \in M$: c_i^g = calculate the center of gravity of c
14. Remove from M the components for which average pixels intensity in the original image I around position indicated by c_i^g is smaller than 0.2
15. $\forall c_i \in M$: construct from I a rectangular ROI with size 31×31 pixels, centered around c_i^g

Fig. 9. The algorithm for detection of Regions if Interest in a mammogram image

References

1. L. J. Warren-Burhenne, S. A. Wood, C. J. D'Orsi, S. A. Feig, D. B. Kopans, K. F. O'Shaughnessy, E. A. Sickles, L. Tabar, C. J. Vyborny, R. A. Castellino, Potential contribution of computer-aided detection to the sensitivity of screening mammography, Radiology 215 (2000) 554–562.
2. S. M. Astley, F. J. Gilbert, Computer-aided detection in mammography, Clinical Radiology 59 (2004) 390–399.
3. J. A. Baker, J. Y. Lo, D. M. Delong, C. E. Floyd, Computer-aided detection in screening mammography: Variability in cues, Radiology 233 (2004) 411–417.
4. M. Heath, K. Bowyer, D. Kopans, R. Moore, P. Kegelmeyer, The digital database for screening mammography, in: The Proceedings of the Fifth International Workshop on Digital Mammography, Medical Physics Publishing, Madison, WI, 2000, pp. 662–671.
5. C. Cortes, V. Vapnik, Support vector networks, Machine Learning 20 (1995) 273–297.
6. H. Cheng, X. Cai, X. Chen, L. Hu, X. Lou, Computer-aided detection and classification of microcalcifications in mammograms: a survey, Pattern Recognition 36 (2003) 2967–2991.
7. B. Zheng, W. Qian, L. P. Clarke, Digital mammography: Mixed feature neural network with spectral entropy decision for detection of microcalcifications, IEEE Transactions on Medical Imaging 15 (1996) 589–587.
8. I. El-Naqa, Y. Yang, M. Wernick, N. Galatsanos, R. Nishikawa, A support vector machine approach for detection of microcalcifications, IEEE Transactions on Medical Imaging 21 (12) (2002) 1552–1563.
9. L. Wei, Y. Yang, R. M. N. and Y. Jiang, A study on several machine-learning methods for classification of malignant and benign clustered microcalcificationsi, IEEE Transactions on Medical Imaging 24 (2005) 371–380.
10. T. Arodz, M. Kurdziel, E. O. D. Sevre, D. A. Yuen, Pattern recognition techniques for automatic detection of suspicious-looking anomalies in mammograms, Computer Methods and Programs in Biomedicine 79 (2005) 135–149.
11. G. Lemaur, K. D. J. DeConinck, Highly regular wavelets for the detection of clustered microcalcifications in mammograms, IEEE Transactions on Medical Imaging 22 (2003) 393–401.
12. P. Heinlein, J. Drexl, W. Schneider, Integrated wavelets for enhancement of microcalcifications in digital mammography, IEEE Transactions on Medical Imaging 22 (2003) 402–413.
13. T. C. Wang, N. B. Karayiannis, Detection of microcalcifications in digital mammograms using wavelets, IEEE Transactions on Medical Imaging 17 (1998) 498–509.
14. T. Netsch, H. O. Peitgen, Scale-space signatures for the detection of clustered microcalcifications in digital mammograms, IEEE Transactions on Medical Imaging 18 (1999) 774–786.
15. W. J. Veldkamp, N. Karssemeijer, Normalization of local contrast in mammograms, IEEE Transactions on Medical Imaging 19 (7) (2000) 731–738.
16. M. Poissonier, J. M. Brady, Noise equalization, film screen artifacts and density representation, in: M. Yaffe (Ed.), Proceedings of the Fifth International Workshop on Digital Mammography, Medical Physics Publishing, Madison, WI, 2001, pp. 605–611.
17. R. Highnam, M. Brady, B. Shepstone, A representation for mammographic image processing, Medical Image Analysis 1 (1996) 1–18.
18. R. Zwiggelaar, S. M. Astley, C. R. Boggis, C. J. Taylor, Linear structures in mammographic images: Detection and classification, IEEE Transactions on Medical Imaging 23 (2004) 1077–1086.

19. C.-M. Chang, A. Laine, Coherence of multiscale features for enhancement of digital mammograms, IEEE Transactions on Information Technology in Biomedicine 3 (1999) 32–46.
20. N. Pandey, Z. Salcic, J. Sivaswamy, Fuzzy logic based microcalcification detection, in: B. W. et. al (Ed.), Proceedings of the IEEE Neural Networks for Signal Processing Workshop X, IEEE Press, 2000, pp. 662–671.
21. H. Li, K. Liu, S. Lo, Fractal modeling and segmentation for the enhancement of microcalcifications in digital mammograms, IEEE Transactions on Medical Imaging 16 (1997) 785–798.
22. T. Arodz, M. Kurdziel, T. Popiela, E. O. D. Sevre, D. A. Yuen, Detection of clustered microcalcifications in small field digital mammography, Computer Methods and Programs in Biomedicine 81 (2006) 56–65.
23. J. Drexi, P. Heinlein, W. Schneider, MammoInsight computer assisted detection: Performance study with large database, in: Bildverarbeitung fur die Medizin: Algorithmen, Systeme, Anwendungen. Proceedings des Workshops vom 9.-11. Marz 2003 in Erlangen, Springer, 2003, pp. 101–105.
24. S. Sentelle, C. Sentelle, M. Sutton, Multiresolution-based segmentation of calcifications for the early detection of breast cancer, Real-Time Imaging 8 (3) (2002) 237–252.
25. J. Jiang, B. Yao, A. Wason, A genetic algorithm design for microcalcification detection and classification in digital mammograms, Computerized Medical Imaging and Graphics 31 (1) (2007) 49–61.
26. C. Garcia-Orellana, R. Gallardo-Caballero, M. Macias-Macias, H. Gonzalez-Velasco, Svm and neural networks comparison in mammographic cad, in: 29th Annual International Conference of the IEEE Engineering in Medicine and Biology Society, 2007, pp. 3204–3207.
27. Y. Sun, C. Babbs, E. Delp, Full-field mammogram analysis based on the identification of normal regions, 2004, pp. 1131–1134.
28. J. Lo, M. Gavrielides, M. Markey, J. Jesneck, Computer-aided classification of breast microcalcification clusters: Merging of features from image processing and radiologists, in: Medical Imaging 2003: Image Processing, Vol. 5032 of Proceedings of SPIE, SPIE, 2003, pp. 882–889.
29. P. Zhang, B. Verma, K. Kumar, A neural-genetic algorithm for feature selection and breast abnormality classification in digital mammography, in: IEEE International Joint Conference on Neural Networks, 2004, pp. 2303–2307.
30. R. Panchal, B. Verma, Classification of breast abnormalities in digital mammograms using image and bi-rads features in conjunction with neural network, EEE International Joint Conference on Neural Networks (2005) 2487–2492.
31. S. Mallat, A theory for multiresolution signal decomposition: The wavelet representation, IEEE Transactions on Pattern Analysis and Machine Intelligence 11 (1989) 674–693.
32. A. Cohen, Biorthogonal wavelets, in: C. K. Chui (Ed.), Wavelets: A Tutorial in Theory and Applications, Academic Press, San Diego, CA, 1992, pp. 123–152.
33. R. M. Haralick, Textural features for image classification, IEEE Transactions on Systems, Man, and Cybernetics SMC-3 (1973) 610–621.
34. S. Mitra, T. Acharya, Data Mining: Multimedia, Soft Computing and Bioinformatics, Wiley-Interscience, Hoboken, NJ, 2003.
35. J. MacQueen, Some methods for classification and analysis of multivariate observations, in: Proceedings of the Fifth Berkeley Symposium on Mathematical Statistics and Probability, University of California Press, Berkeley, 1967, pp. 281–297.
36. K. Boryczko, M. Kurdziel, Approximate clustering of noisy biomedical data, to appear in: Proceedings of the International Conference on Computational Science 2008 (ICCS 2008), Krakow, PL, 2008.
37. D. B. Kopans, Breast Imaging 2nd edn., Lippincott Williams & Wilkins, Philadelphia, 1998.
38. A. P. Dhawan, Y. Chitre, C. Kaiser-Bonasso, M. Moskowitz, Analysis of mammographic microcalcifications using gray-level image structure features, IEEE Transactions on Medical Imaging 15 (1996) 246–259.
39. H.-P. Chan, B. Sahiner, K. L. Lam, N. Petrick, M. A. Helvie, M. M. Goodsitt, D. D. Adler, Analysis of mammographic microcalcifications using gray-level image structure features, Medical Physics 25 (1999) 2007–2019.
40. F. Schmidt, E. Sorantin, C. Szepesvari, E. Graif, M. Becker, H. Mayer, K. Hartwagner, An automatic method for the identification and interpretation of clustered microcalcifications in mammograms, Physics in Medicine and Biology 44 (1999) 1231–1243.
41. D. P. Chakraborty, Maximum likelihood analysis of free-response receiver operating characteristic (froc) data, Medical Physics 16 (4) (1989) 561–568.
42. N. Karssemeijer, Adaptive noise equalization and recognition of microcalcification clusters in mammograms, International Journal of Pattern Recognition and Artificial Intelligence 7 (1993) 1357–1376.
43. N. C. Yarlagadda, K. W. Bowyer, R. Li, Baseline comparison of microcalcification detection algorithms, in: M. Yaffe (Ed.), Proceedings of the Fifth International Workshop on Digital Mammography, Medical Physics Publishing, Madison, WI, 2001.
44. L. Ries, M. Eisner, C. Kosary, B. Hankey, B. Miller, L. Clegg, A. Mariotto, E. Feuer, E. B., SEER Cancer Statistics Review, 1975–2002, National Cancer Institute, Bethesda, MD, 2004.
45. T. W. Freer, J. M. Ulissey, Screening mammography with computer-aided detection: Prospective study of 12,860 patients in a community breast center, Radiology 220 (3) (2001) 781–786.
46. H.-P. Chan, L. T. Niklason, D. M. Ikeda, K. L. Lam, D. D. Adler, Digitization requirements in mammography: Effects on computer-aided detection of microcalcifications, Medical Physics 21 (1994) 1203–1211.
47. K. J. McLoughlin, P. J. Bones, N. Karssemeijer, Noise equalization for detection of microcalcification clusters in direct digital mammogram images, IEEE Transactions on Medical Imaging 23 (3) (2004) 313–320.
48. S. Yu, L. Guan, A cad system for the automatic detection of clustered microcalcifications in digitized mammogram films, IEEE Transactions on Medical Imaging 19 (2000) 115–126.

49. R. N. Strickland, H. I. Hahn, Wavelet transforms for detecting microcalcifications in mammograms, IEEE Transactions on Medical Imaging 15 (1996) 218–229.
50. K.-R. Muller, S. Mika, G. R. K. Tsuda, B. Scholkopf, An introduction to kernel-based learning algorithms, IEEE Transactions on Neural Networks 12 (2001) 181–201.
51. C. Burges, A tutorial on support vector machines for pattern recognition, Knowledge Discovery and Data Mining 2 (1998) 121–167.

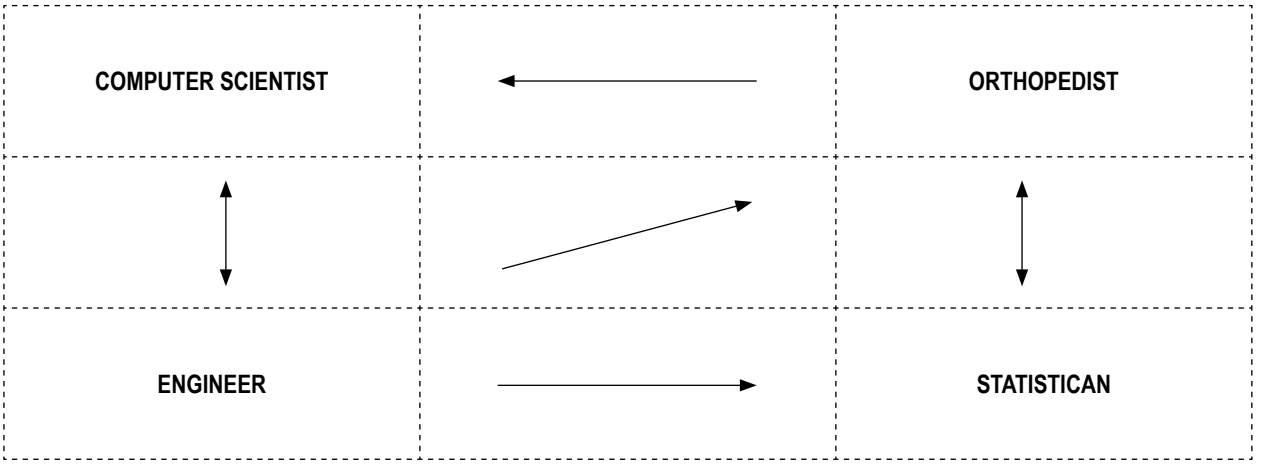

BIO-ALGORITHMS AND MED-SYSTEMS
JOURNAL EDITED BY MEDICAL COLLEGE – JAGIELLONIAN UNIVERSITY
Vol. 3, No. 6, 2007, pp. 23-26

MAGNETIC HEART VECTOR AND ITS POTENTIAL USE IN MAGNETOCARDIOGRAPHY

Stanisław Micek[1], Mieczysław Pasowicz[2], Zenon Nieckarz[1],

e-mail: ufmicek@cyf-kr.edu.pl
[1] Institute of Physics Jagiellonian University, ul. Reymonta 4, 30-059 Kraków
[2] John Paul II Hospital, ul. Prądnicka 80, 31-202 Kraków

Abstract: A new method of magnetocardiograms presentation bas been developed. The basis of the method is the average magnetic field vector calculated from the map of extracorporeal magnetic field of the heart, generated by cellular ionic currents. An ion current source similar to the shape of "W" letter is defined. The average magnetic field vector (AMFV) from this source is calculated and plotted as a form of trajectory. The trajectory shape contains serial information about electrical functioning of the heart. It may be used for diagnostics of the ion conduction in the heart.

Key words: AMFV, heart dignostic, vector trajectory, MCG criteria

Streszczenie: Przedstawiono nową metodę obrazowania wyników magneto-kardiograficznych. Podstawą metody są obliczenia średniego wektora pola magnetycznego wyznaczonego z mapy zewnętrznego pola magnetycznego serca generowanego przez jonowe prądy komórkowe. Określono źródło prądów o kształcie podobnym do litery „W". Średni wektor pola magnetycznego (AMFV) z tego źródła jest obliczony i wykreślony w formie trajektorii. Kształt trajektorii zawiera szeregowe informacje o elektrycznym działaniu serca. Może być on użyty w celu diagnostyki przewodnictwa jonowego serca.

Słowa kluczowe: średni vektor magnetyczny, diagnostyka serca, trajektoria wektorowa, kryteria w magnetokardiografii

Introduction

The magnetocardiography (MCG) is a non-invasive mapping technique to register the extracorporeal magnetic field of the heart, generated by cellular ionic currents. The electric ionic current creates not only electric potential, but also a magnetic field. This weak magnetic field from the heart can be measured with a superconducting quantum interference device (SQUID) utilised as an ultra sensitive magnetic field sensor. Typical mapping of the magnetic field is conducted with a multi-channel SQUID system. Baule and McFee introduced the concept of the magnetic heart vector in 1970 [1]. Various studies have been conducted to calculate the vectormagnetocardiogram, in which the heart is considered as a moving magnetic dipole. Till now some parameters of the vectormagnetocardiogram have been defined as the criteria for ischemia [2] during different time intervals, particularly at the T-wave. Typically four parameters for characterization of CAD are used: direction of the vector (defined from plus pole to minus pole), change in the angle of this vector, change in the distance between plus and minus poles, and the change in the ratio of the pole strengths. Some criteria are based on the identification of rapid changes in indicated vector parameters [2]. The healthy subject displays a very stable vector behavior, with only slow, slight changes in the magnetic field vector. The single parameter contains a limited number of information and is insufficient for full diagnosis of a suspected acute coronary syndrome (ACS). Movement of the single parameter like AMFV in a various phase of the heart action may point at the place of a disease [3].

There are some advantages of MCG over ECG. In MCG we measure the electric activation of the whole cardiac muscle, whereas in ECG we have information about anterior surface of a muscle. A combination of electric and magnetic measurements (i.e. ECG and MCG) gives a better diagnostic performance than any other method alone with the same number of diagnostic parameters, because the number of independent measurement doubles.

The main aim of this paper is to catch up the movement of the average magnetic field (trajectory) during QRS-wave by simulation of the ion current along a given shape. Presented modeling is based on a simple ion current propagation in the heart along two "U" branches (left and right) according to "W" letter. Results of calculations are de facto qualitative, existing in the form of a vector trajectory. At this level the shape of "W" letter is not essential because no numerical output data are calculated.

Average Magnetic Field Vector (AMFV)

The MCG measures the magnetic vector field. Therefore, MCG measurements should provide a vector description. In MCG, the normal component of the magnetic field B_z, which is perpendicular to the chest wall, is usually measured. In con-

tour map of B_z a two-pole pattern having positive and negative poles is produced, and the separation between the poles defines the dipole vector length. However, our definition of AMFV is different than used in vectoromagnetocardiography (VMCG) where the vector magnetic field with three orthogonal components is used.

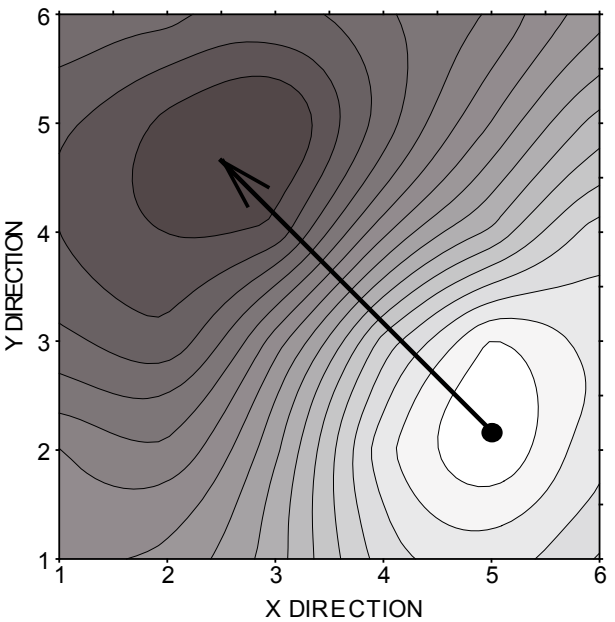

Fig. 1. Typical B_z magnetic isofield map and the dipole vector in X-Y plane of the hearth around thorax as results of the "W" model calculation

The dipole coordinates are calculated in detector distance units. The weighted average position value of the positive pole signal for MCG (center of gravity) and the value of weighted average negative pole signal define our average dipole magnetic heart vector according to the formula:

$$\mathbf{R} = \frac{\sum_i \left(B_Z^+\right)_i * \mathbf{r}_i}{\sum_i \left(B_Z^+\right)_i} - \frac{\sum_i \left(B_Z^-\right)_i * \mathbf{r}_i}{\sum_i \left(B_Z^-\right)_i} \qquad (1)$$

where: B_z is the magnetic field in direction Z and at position $\mathbf{r}_i$, + stand for the positive value of the magnetic field, – is for the negative. Typical analysis is made only in a one X, Y plane for r_z = 1.5 detector distance. Vector movements contain serial information similar to the ECG, but indicate an electrical current magnetic activity of the heart.

The mapping has usually been done with a grid. The most popular grid, introduced by Malmivo, Saarinen, and Siltanen (1973) [4] includes 6x6 multichannel SQUID locations on the anterior thoracic wall. This grid has become known as the "standard grid" [5], [6], and was used in the present calculation. Calculated z-component of magnetic field of the heart typically contains one maximum in a plus pole and one in a minus pole. The isofield map is presented in Fig.1 together with the vector defined by equation (1). In the case when one positive pole is present, the formula (1) identifies an average negative background as a negative pole. Calculated vector may change rapidly.

Model of the "W" source

The propagation of a current signal from AV node is provided by a specialised conduction system. A current separates into two bundle branches propagating along each side of the septum, constituting right and left branches. Two different volume conductor shapes of a current source like "U" letter were used in the study. They are forming the "W" letter. In this method many electric current elements distributed in a volume conductor are replaced by using one-point time data in one of the "U" branch without prescribing the number of dipoles. Two average electric current sources from both "U" shapes are applied simultaneously in the calculation.

To analyse a magnetic heart dipole movement in the detail through simulation we use the "W" model. The model should represent a hypothesis regarding physiological observations. The propagation along two "U" branches forming "W" letter is used as a main source of magnetic field signal. The magnetic field originating from an electrical current source in the volume can be calculated from the Biot-Savart law:

$$\mathbf{B}(\mathbf{r}) = \frac{\mu_0}{4\pi} \int_{\mathbf{r}'} \mathbf{J}_{\mathbf{tot}}(\mathbf{r}') \times \frac{\mathbf{r} - \mathbf{r}'}{|\mathbf{r} - \mathbf{r}'|^3} \mathbf{dr}' \qquad (1)$$

where μ_0 is the permeability of the free space, **r** is the measurement position, **r'** is the source position, $\mathbf{J}_{\mathbf{tot}}$ is the total volume electrical current. The integration is taken over whole source volume.

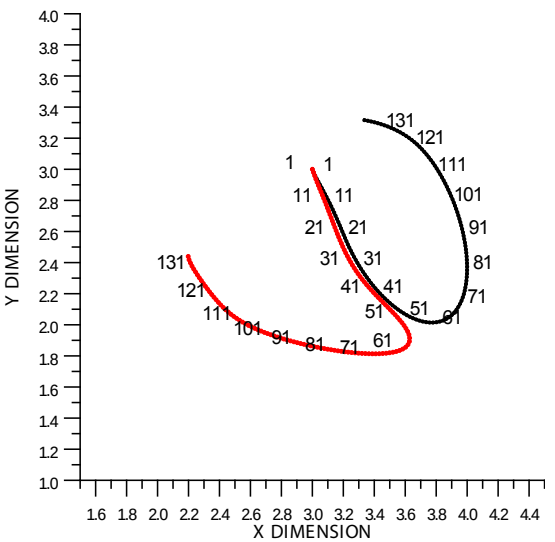

Fig. 2. The shape of two conductivity branches in "W" model. Numbers indicate the time scale of an electrical current flow in relative units.

The conductivity pathway in a human heart was received by 10-th order polynomial fit to the cross section of a heart. Numbers shown in Fig. 2 indicate a time scale of an ion current propagation in relative units. The differences of the conductivity pathway in the human body cause accumulation of charge on interfaces, which act as secondary sources altering a current distribution. In our model it is replaced by a radial current component directed to the middle of "U". This simulates also the ventricular activation from the inner wall of the left ventricle and proceeds radically toward the epicardium.

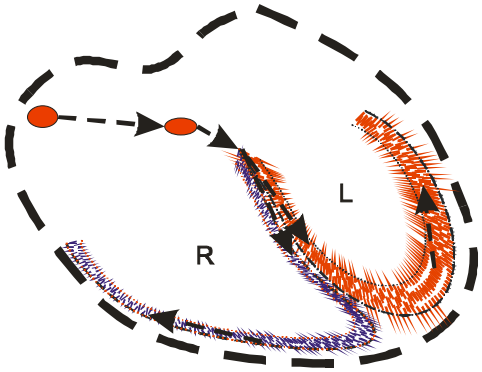

Fig. 3. The "W" shape of volume conductor and the cardiac electrical current flow with activation sequence.

In our model a volume current $\mathbf{J}_{tot}$ was chosen in radial direction relative to the middle of each "U" part separately. The value of the ion current is not important for magnetic vector calculations. Location of the magnetic field maximum in Fig. 1 remains unchanged. Only direction of ion propagation and the wall thickness are essential. The free wall of left ventricular and the septum are in Fig. 3 much thicker than the right ventricular wall.

Outcomes

The temporal information of the dipole magnetic vector may be plotted in a form of curve. Numbers surrounding the vector trajectory in Fig. 4 describe a time scale introduced in Fig. 2. The dipole vector is turning a loop moving anticlockwise in the circle for the left part "L" of "U' and for "R" part in clockwise direction. The final result of a "W" shape is a superposition of both "U" signals. A higher current in "L" shape than in "R" shape is displayed in the superposition as anticlockwise circle.

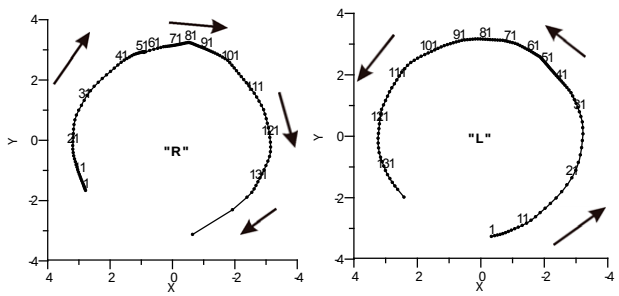

Fig. 4. The dipole magnetic vector generated by the left "U" part of "L" as is drawn in Fig. 2 (left picture) and for the part "R" (right). As it is drawn in Fig. 2 time scales (in relative units) are printed as numbers placed close to the line. The vector loop in the left picture turns anticlockwise simulating "L" and is in opposite direction to the loop in the right picture for "R".

Various activation processes were used in the calculation designed for diverse signal propagation. The smaller thickness of the left line in "L" wall change dramatically average vector trajectory. The trajectory in the right picture (in Fig. 5) is turning back when activation is passing through right side of "L" line.

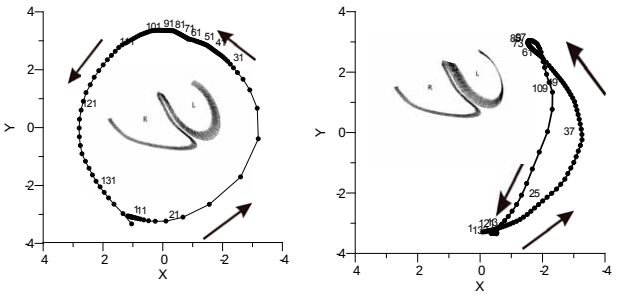

Fig. 5. Average dipole magnetic vectors for two different thickness of the left "L" part of "U". The "W" picture is also presented in the middle. The trajectory of vector for thin wall (on the right picture) makes a narrow loop easy for identification. This may resemble a smaller ion current from the "L" part at the end of the depolarisation (coronary artery disease CAD).

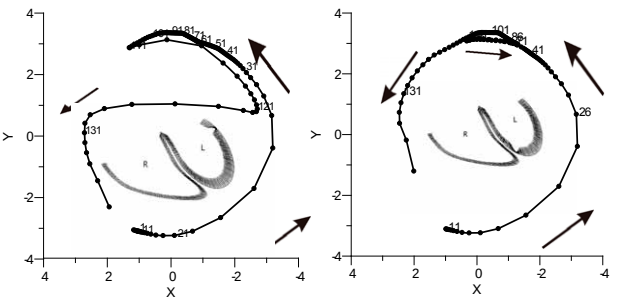

Fig. 6. Average dipole magnetic vectors for two different local changing the thickness of the left "L" part of "U" wall. The "W" picture is also present the middle. The vector trajectories are different and may indicate the place of the "U" where changes are made.

Defects in the ion current propagation (direction and velocity) show new loops in the average vector trajectory. Defects shown in Fig. 6 reflect time of occurrence in vector trajectory observed as a rapid change in the vector angle.

Results of measurements

With the magnetocardiograf CardioMag Imaging Inc. containing 9 SQUID detectors with four measurements in various positions it was possible to measure the magnetic field in 36 points. For triggering purposes ECG data were recorded sequentially at four well-defined bed positions during 90 seconds in each position with frequency 1 kHz. The interspacing of the SQUID sensors was 4 cm. The area of 20 cm x 20 cm over the chest was covered.

The software calculates one averaged cardiac cycle for each of the 36 positions. A typical magnetic field vector for a healthy subject is shown on Fig. 7. For the QRS wave (left) AMFV turns anticlockwise opposite to the T-wave, which presents a clockwise direction. Points with higher density indicate slower propagation of the ion current in the detector plane.

In Fig. 7, and 8 all the points on the vector trajectory are in 1 ms time space. The higher density of points indicates slower vector movement. In the normal heart a higher density of points in QRS-wave is observed a few milliseconds after R point. For T-wave a higher density occur close to maximum of T-wave.

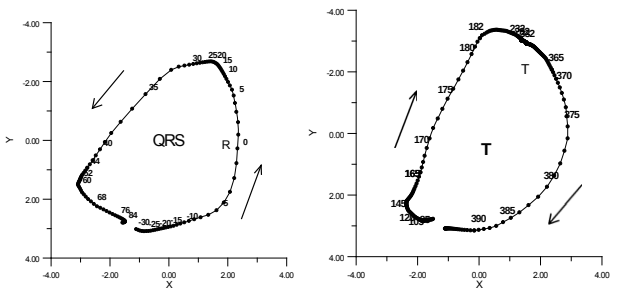

Fig. 7. Trajectories of the average magnetic field vector AMFV for a healthy subject during QRS (left) and T (right) wave is moving in the circle in an opposite direction. Points are plotted in 1 ms time space relative to the R-wave.

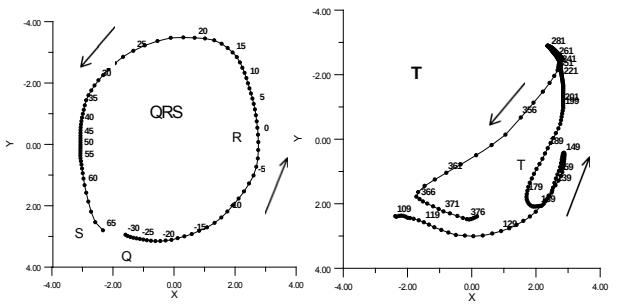

Fig. 8. The trajectory of AMFV for T-wave of a second subject being after infraction is very complicated (right picture). AMFV turns for T-wave anticlockwise showing lower not homogenous current in the left ventricle.

The trajectory of magnetic field vector for a subject after infarction presents various phenomena (Fig. 8). Points in QRS are equidistant. Some correspondence with Fig. 7 in QRS (left picture) is only observed in the circular shape of the trajectory. The magnetic vector velocity observed as a distance between points indicates almost constant velocity of vector on trajectory in Fig.8. In the model trajectory calculations in Fig. 5 we notice the highest vector velocity close the maximum in R wave what is not the case shown in Fig. 8. This phenomenon will be explained in future publications where an angioplasty intervention is improving the ion conductivity. The trajectory for T-wave makes few turns showing various conductivity of the left chamber wall.

Conclusion

In this paper, the numerical method of solving the bioelectromagnetic forward problem is presented. To our knowledge, the method defines at the first time the average magnetic field vector for ion movement during QRS-wave or T-wave and the vector trajectory. The method uses all magnetic field poles seen in the detection plane. The "W" conductor modeling in this study is very simplistic, but nevertheless, the model is related to the real anatomical structures of the human body.

The description of the dipole model above, disregards the bulk magnetisation of the sample, so this expression accounts only for the field generated by the flaw. Not all myocardiac cells in the heart show the same response to activation. Generally, two classes of cell responses are distinguished. In the model we have the slow (myocardiac cells) reaction and the fast (sodium channels) response. They are identified in calculations as the "W" current and the radial current, respectively.

After depolarisation phase observed during QRS-complex, in the repolarisation process all cells return to his resting state. We can expect that direction of magnetic field movement in repolarisation be opposite to the depolarisation. Instead of anticlockwise movement in QRS-wave we have clockwise vector movement during a T-wave. Slower depolarization process is indicating more detailed structure in the vector trajectory. As a main tool indicating some defects in the ion current propagation, the rapid change in an average magnetic field vector may be used. Rapid changes in the velocity or in the direction of average vector indicate some obstacles existing during ions flow. The occurrence time of changes in a speed of magnetic vector movement shows a position of defects during ions conductivity.

References

1. Baule G. M, McFee R.: Detection of the magnetic field of the heart, Am. Heart J., 66(7) 95-6,1963 /Baule G. M, McFee R.: The magnetic heart vector, Am. Heart J., 79(2), 223-36, 1970.
2. Jai-Wun P., Hill P. M., Namsik Ch., Hugenholtz P. G., and Jung F.: Magnetocardiography Predicts Coronary Artery Disease in Patients with Acute Chest Pain, A.N.E, The Annals of Noninvasive Electrocardiology, 10, 312-323, July 2005.
3. Micek S., Owsiak D., Surdacki A.: Average magnetic heart vector calculated from cellular ionic currents, Bio-Algorithms and Med.-Systems, in this volume.
4. Malmivo J. A., Saarinen M., Siltanen P.: A clinical method in magnetocardiography, In Digest X Internat. Conf. Med. Biol. Eng., Vol. I, ed. A. Albert, W. Helbig, p. 251, Dresden 1973.
5. Karp P.: Cardiomagnetism in Biomagnetism, Proc. Third Internat. Workshop On Biomagnetism, Berlin, May 1980, ed. SN Erme, H-D Hahbohm, H. Lubbig, p. 251, Dresden 1981.
6. Seppanen M., Katila T., Tomisto T., Varpula T., Duret D., Karp P.: Measurements of the biomagnetic fields using multichannel superconducting magnetometer techniques, Il Nuovo Cim., 2D 166-74, 1974.

PHYSICIST	⟷	CARDIOLOGIST

BIO-ALGORITHMS AND MED-SYSTEMS
JOURNAL EDITED BY MEDICAL COLLEGE – JAGIELLONIAN UNIVERSITY
Vol. 3, No. 6, 2007, pp. 27-29

AVERAGE MAGNETIC HEART VECTOR CALCULATED FROM CELLULAR IONIC CURRENTS

STANISŁAW MICEK[1], DAWID OWSIAK[1], ANDRZEJ SURDACKI[2]

[1] Institute of Physics Jagiellonian University
ul. Reymonta 4, 30-059 Kraków
[2] 2nd Department of Cardiology, Jagiellonian University
ul. Kopernika 17, 31-501 Kraków

Abstract: A two-dimensional computer model of the heart electrical activity, based on the formalism proposed by Hodgkin and Huxley, was used to calculate magnetocardiograms. Presented calculations have been aimed at the average magnetic field vector (AMFV) [1] obtained from the map of extracorporeal magnetic field generated by the heart, whose underlying cause are cellular ionic currents. The calculation of magnetic field was performed for ionic currents within of a set of myocardial cells. In a normal heart the trajectory of AMFV accompanying QRS complex computed from the model mimics a circle rotating anticlockwise. Abnormal trajectories of AMFV associated with some cardiac pathologies have been generated from the model. If properly validated in clinical conditions, measurements of AMFV may be potentially helpful for diagnostic purposes.

Keywords: heart modeling, MCG, heart vector, heart cell system, Hodgkin Huxley method

Streszczenie: Do obliczenia magnetokardiogramów użyto dwuwymiarowego modelu komputerowego elektrycznej aktywności serca bazującego na formalizmie utworzonym przez Hodgkina i Huxleya. Celem obliczeń był średni wektor pola magnetycznego (AMFV) otrzymany z mapy zewnętrznego pola magnetycznego generowany przez przepływ jonów w poszczególnych komórkach mięśnia serca. Trajektoria AMFV dla normalnego serca w czasie trwania zespołu QRS zapisu EKG obliczona z modelu przyjmuje kształt kolisty z rotacją w kierunku przeciwnym do ruchu wskazówek zegara. Na podstawie modelu przedstawiono przykładowe zaburzenia trajektorii AMFV towarzyszące określonym zaburzeniom serca. O ile wartość omawianej metody zostanie potwierdzona w warunkach klinicznych, pomiar AMFV może by potencjalnie użyteczny dla celów diagnostycznych.

Słowa kluczowe: modelowanie serca, MKG, wektor serca, komórki serca, metoda Hodgkina Huxleya

Introduction

Anomalous propagation of electrical impulses in the myocardial tissue occurs frequently in the course of cardiovascular disorders. Almost every part of myocardial tissue can become the origin of abnormal ectopic activity. Atrial fibrillation or flutter, monomorphic and polymorphic ventricular tachycardia is associated with abnormalities of impulse generation and propagation. In search of the basis of these pathologies, ionic currents within single myocardial cells should be investigated in physiological and pathological conditions, which however poses methodological difficulties. Vice versa, modeling of electrical and magnetic activity of the heart provides insight into abnormalities at the cellular level from measurements by means of noninvasive techniques.

The aim of the present study was to calculate the average magnetic field vector movement (trajectory) accompanying QRS complex (by ECG) using a cellular model simulation based on the formalism proposed by Hodgkin and Huxley [2].

Average magnetic field vector AMFV

In a contour map of the magnetic field (X,Y plane) we calculate only B_z component. This component has a two-pole pattern having positive and negative poles, and the separation between these poles defines the dipole vector length. Dipole coordinates of AMFV are calculated in the units of distance between detectors (4 cm). Additionally, an angle relative to the origin of the measurement grid is also calculated. The weighted average position value of a positive signal for MCG (center of gravity) and the value of weighted average negative signal define our average dipole magnetic heart vector [1]. AMFV trajectory contains serial information similar to ECG but it indicates the magnetic activity of the heart. Calculated z-component of magnetic field of the heart contains typically one maximum in a plus pole and one in a minus pole. .

Modeling of magnetic field from heart cells system (HCS)

Presented model [3], [4] of the heart electrical activity assumes four different cellular ionic currents and three kinds of

gate variables. The condition reconstructed by the model allows linking the cells into structures thus imitating the real heart stimulation systems.

The resting potential of sinoatrial node cells is about –60 mV and is higher than the potential of other heart cells. The temporal membrane potential is connected with ionic currents by the following equation:

$$-C\frac{dV}{dt} = I_{Ca} + I_{Na} + I_{K1} + I_{K2} \quad (1)$$

where : **C** – cell capacity , **V** – membrane potential, $\mathbf{I}_{on}$– ionic currents. These currents can be described by the following equations:

$$I_{Ca} = g_{Ca} d\, f (V - V_{Ca}) \ , \ I_{Na} = g_{Na} m^3 h (V - V_{Na}), \quad (2)$$

$$I_{K1} = g_{K1} \frac{1 - \exp\left[\frac{V_{K1} - V}{S_{K1}}\right]}{1 + \exp\left[\frac{V - V'_{K1}}{S_{K1}}\right]}, \quad I_{K2} = \frac{g_{K2}(V - V_{K2})}{1 + \exp\left[\frac{V_{K2} - V}{S_{K2}}\right]}$$

where: V_{ion} – equilibrium potential of each ion; d, m – activate variables of each channel; f,h closing variables of each channel; g_{ion} –conductance of each channel. Notice that d, m, f, h are time- and membrane potential-dependent functions. All of parameters value can be found in calculations presented by Owsiak and others [3], [4].

After formulating the equations, a delimitation of all constant parameters (like S_{ion}) should be done in order to obtain a proper shape of action potential similar to that of real cells [5]. These parameters include such aspects as ion channel conductance and equilibrium potentials. Moreover, as a model test a comparison should be used between the cell model's responses to external influences versus a real experiment performed on living cardiac cells [5]. The model is built from 30 x 40 = 1200 clusters, which can be treated as a set of heart cells with the same properties and nearly the same membrane potential at a given time. Those clusters are placed on the two-dimensional matrix in a manner that represents the geometry of heart muscle cross-section.

Single cluster simulation tells us about the resting and action potential of cells inside the cluster. To build an extended structure composition of many clusters from which one can act on another, the definition of linkage between clusters should be made. For the aim to be reached, an additional current should be introduced into the main equation (Eq.1). This current should be proportional to the potential difference between external membrane surfaces of two joined clusters (i,j):

$$I_C^{ij} = g_C^{ij} \Delta V_{ij} \quad (3)$$

where: ΔV_{ij} – difference of the potentials on external membrane surface from two neighbour clusters – i,j, g_c – coupling constant with a value 0.03 nS/pF . Such cell linkage was tested by comparing an outcome of computer simulations with results of the real experiments performed on rabbit sinoatrial node cells and published by Verheijck and others [5].

The following six different kinds of heart cells are important for correct heart electrical activity simulations:

a) Sinoatrial node cells (SA)
b) Atrioventricular node cells (AV)
c) His bundle cells (PH)
d) His bundle branches cells
e) Purkinje fibres cells
f) Myocardial cells

Here, the first five kinds of cells (from points "a" to "e"), build the pacemaker and conductance system, which is responsible for generation and proper propagation of the wave depolarization in the heart. The last type from the mentioned above ("f") represents working cells, which builds the prevalent mass of the heart. The model can generate correctly the membrane potential run.

The magnetic field originating from an electrical current source of (i,j) cell in the total volume can be calculated from the Biot-Savart equation.

$$\mathbf{B}(\mathbf{r}) = \frac{\mu_0}{4\pi} \sum_{ij} \int_{\mathbf{r}'} \mathbf{J}_{tot}^{ij}(\mathbf{r}'_{ij}) \times \frac{\mathbf{r} - \mathbf{r}'_{ij}}{\left|\mathbf{r} - \mathbf{r}'_{ij}\right|^3} \mathbf{dr}'_{ij} \quad (4)$$

where μ_0 is the permeability of the free space, **r** is the measurement position, **r'** is the source position, $\mathbf{J}_{tot}^{j}$ is the total volume electrical current. Integration is taken over whole source volume as a sum of all active cells.

The shape of a calculated magnetic vector trajectory does not depend on the scale of an ion source. Rotation of the heart as a source rotates also the trajectory. Limited number of active cells introduces some kind of quantum effects and almost every few cells are considerable.

AMFV moves comparably in Figures 1-3 from point 1 to 4. Both axes in Figures 1-3 are in relative units. The size of trajectory, but not the shape, depends on a relative position of detection plane in respect to the ion source plane.

In the presence of a necrotic zone in the left or right ventricle AMFV trajectory considerably changes. A detailed analysis of the vector trajectory shows minor changes in the conductivity. Additionally, a fine structure of the calculated trajectory results from a limited number of cells and from a time step used in data presentation.

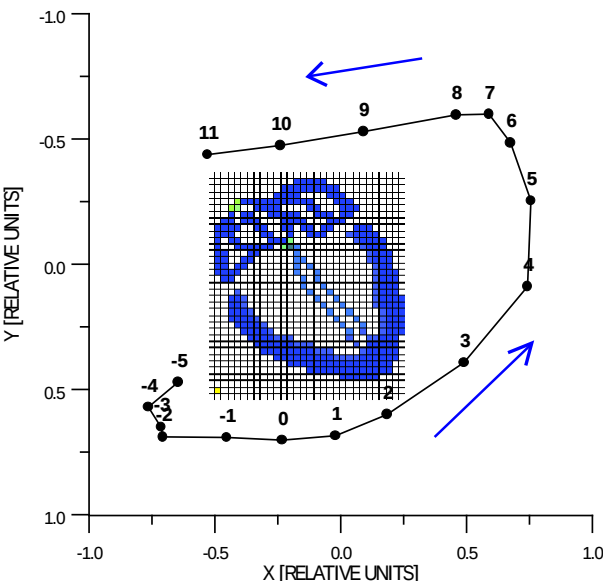

Fig. 1. Average magnetic field vector (AMFV) during the ECG QRS complex – an approximately anticlockwise rotation. A cross-section of the heart with model matrix has been depicted in the middle of the Figure. Points on the trajectory are plotted in every 5 ms. Numbers indicate a time scale with zero at a maximum R wave.

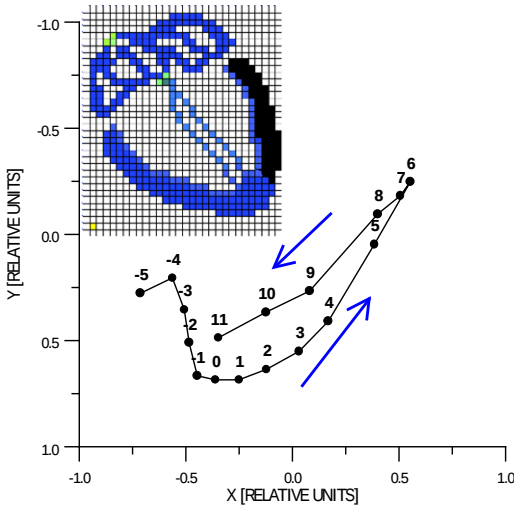

Fig. 2. AMFV trajectory changes the direction to the opposite (point 6) in the presence of a necrotic zone within the left ventricle

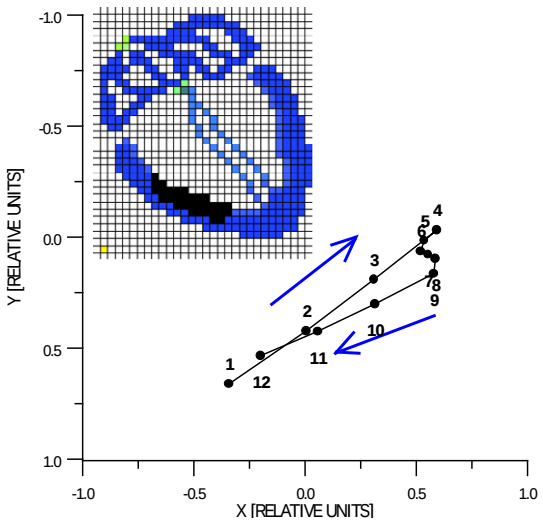

Fig. 3. AMFV trajectory changes the direction (points 4 and 5) in the presence of a necrotic zone within the right ventricle

Conclusion

The use of heart cells system (HCS) to generate various patterns of the AMFV trajectory helps to identify zones of abnormal impulse propagation. In theory, this might be helpful for diagnostic purposes. Extension of presented model to 3D space seems to be a desirable and promising field of research. Nevertheless, more complicated shapes of the vector trajectory require proper clinical validation before it may be proposed as an imaging tool. For the time being, problems with the interpretation of various trajectory patterns remain a major drawback of the AMFV technique.

On the other hand, future studies appear advisable to improve the presented technique. Insofar as electrocardiography has a limited value in diagnosing discrete abnormalities of impulse propagation within the heart, optimizing of the non-invasive investigative approach is of extreme interest for clinicians. Moreover, whereas a dramatic progress has been reached with regard to imaging of ventricular function by means of nuclear magnetic resonance, detailed studies of electrophysiological parameters still require an invasive approach. This supports the relevance of future re-assessment of the usefulness of data obtained from the measurement of heart magnetic fields as an underestimated diagnostic tool.

References

1. Micek S., Pasowicz M., Nieckarz Z.: Magnetic Heart Vector and its Potential Use in Magnetocardiography, Bio-Algorithms and Med.-Systems, in this volume.
2. Hodgkin A.L., Huxley A.F.: A quantitative description of membrane current and its application to conduction and excitation in nerve, J. Physiol. (Lond), 117, 500-544, 1952.
3. Owsiak D., Micek S.: The Computer Model of Heart Electrical Activity, Biocybernetics and Biomedical Enginerring, 25, 41-52, 2005.
4. Owsiak D., Burzyński P., Micek S.: Modelling of the Linked Sinoatrial Node Cells Systems, Structures-Wawes, Biomedical Engineerig, XI, 197-204, 2002.
5. Verheijck E., Wilders R., Joyner R.W., Gold D.A., Kumar R., Jongsma H.J., Bouman L.N., van Ginneken A.C.: Pacemaker synchronisation of electrically coupled rabbit sinoatrial node-cells, J. Gen. Physiol., 1.111, nb 1, 95-112, 1 Jan 1998.

BIO-ALGORITHMS AND MED-SYSTEMS
JOURNAL EDITED BY MEDICAL COLLEGE – JAGIELLONIAN UNIVERSITY
Vol. 3, No. 6, 2007, pp. 31-35

NUMERICAL ANALYSIS OF THE STATES OF STRESSES IN THE UNITS OF ZESPOL TYPE STABILIZER

WOJCIECH WIĘCKOWSKI

Zakład Inżynierii Biomedycznej, Politechnika Częstochowska, Częstochowa,
wieckowski@iop.pcz.czest.pl

Abstract: In the paper state of stress of the ZESPOL plate stabilizer elements of the bridging osteosynthesis has been subjected to the numerical analysis. Calculation have been performed for variable fixing of the bearing element of the stabilizer versus bone in the system loaded respectively with axial force, bending moment in the frontal and sagittal plane and torque moment. Reduced stresses values and normal stresses components in the bearing plate of the stabilizer and bone screws have been determined with FEM simulation. Results obtained from the calculation shows significant influence of the fixing type of the stabilizer versus bone on loading of the individual elements of the joint system and further on its durability and assurance of the proper conditions for bone union.

Key words: osteosynthesis, ZESPOL plate stabilizer, computer simulation

Streszczenie: Przedmiotem badań była analiza numeryczna stanu naprężeń w elementach stabilizatora płytkowego ZESPOL w modelu zespolenia mostującego kości. Obliczenia przeprowadzono dla różnych wariantów utwierdzenia nośnika stabilizatora względem kości, w układzie obciążonym odpowiednio: siłą poosiową, momentem gnącym w płaszczyźnie czołowej i strzałkowej oraz momentem skręcającym. Wyznaczono wartości naprężeń zredukowanych oraz składowych naprężeń normalnych w płytce nośnej stabilizatora oraz wkrętach kostnych z wykorzystaniem MES. Uzyskane wyniki obliczeń wykazują znaczący wpływ sposobu zamocowania stabilizatora względem kości na obciążenie poszczególnych elementów układu zespolenia, a przez co na jego trwałość i zapewnienie odpowiednich warunków do prawidłowego zrostu kostnego.

Słowa kluczowe: osteosynteza, stabilizator płytkowy ZESPOL, symulacja komputerowa

1. Introduction

Plate stabilizers osteosynthesis is one of the optimal fixation methods of the bone fragments in treatment of the most cases of breaking, pseudarthrosis with bone defects and disturbance of bone union of the long bones, i.e. tibia, brachium or anterbrachium. It also becomes a successful alternative to the intermedullary fixation of the femur, especially regarded to the traditional plate fixation, what is acknowledged by the clinical tests [7, 9].

Despite of high effectiveness of the plate stabilizer osteosynthesis method, many complications such as: stabilizer elements failure, lack of breaking healing, septical loosening or faulty fixation of the bone fragments are observed. These complications occur mainly due to the lack of the proper fixation stabilization, mechanical failure or excessive loading of the limb (fig. 1) [1, 3, 7, 9].

Numerous defects of the osteosynthesis extorted the elaboration of new fixing techniques, in which pressure of the plate on a bone surface is eliminated either partially (limited contact plates LC-DCP) or completely (non-contact plate stabilizers ZESPOL, ALTROFIX and POLFIX) [2, 6, 8, 9].

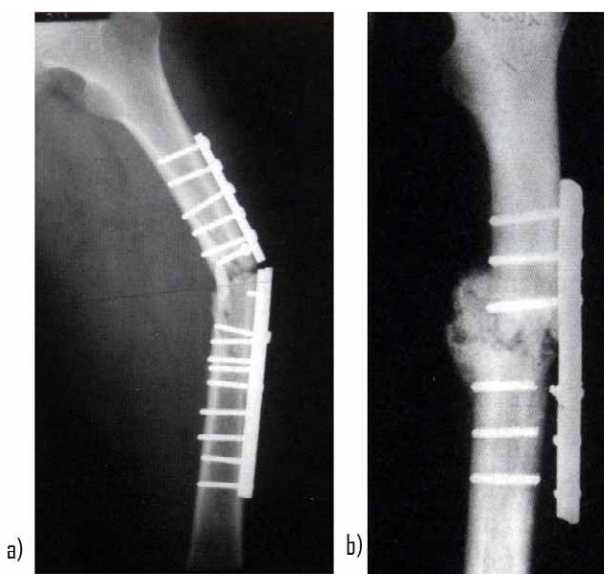

Fig. 1. Destabilization of the fixing: a) plate, b) ZESPOL stabilizer [1, 9]

In a plate stabilizer fixation, by fixed connection of the bearing element and screws, elastic loading transfer and required mobility of bone fragments in a breaking region are obtained, what resulted in providing conditions to consolidation and scar creation.

Plate stabilizer fixation technique, construction of the stabilizer (bearing element dimension – plate, screws diameter and length) as well as its location relative to bone should provide optimal fixing elasticity, and further, proper conditions for bone union [3, 4, 5, 9, 10].

2. Methodology

In the paper, stabilizing system built with symmetrical ZESPOL stabilizer plate, cross section dimensions 16x4,5mm and length 110mm with six holes spacing equals to 32 mm and standard equal to 16mm has been subjected to the evaluation. Stabilizer has been fixed to the bone fragments with standard cortical screws φ=4 mm (fig. 2).

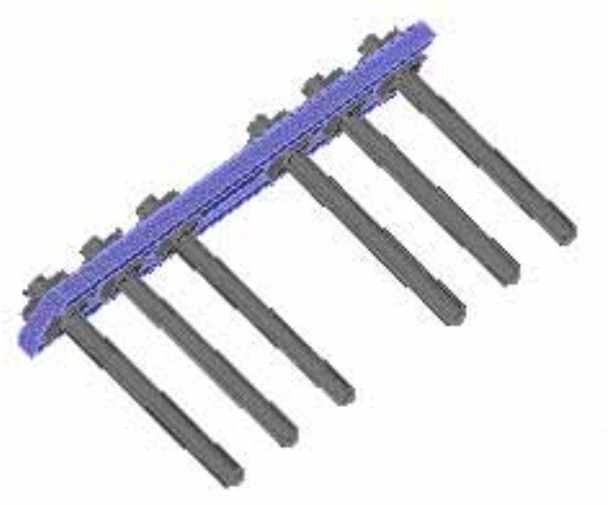

Fig. 2. Geometrical model of ZESPOL stabilizer

Calculation has been performed for a system fixing bridging bones used for bone decrement or its fragmentation resulting from mechanical injury. In the discussed model a fixing stabilizes bone fragments in the distance of 4 mm one from the other, while entire loading is transferred by stabilizer elements.

Discrete model of the stabilizing system has been presented in fig. 3. Digitalization of the system has been performed with use of four nodal finite elements TETRA 4. Rigid fixing of the cross section plane of a bone fragment has been set up, while on an end of the other fragment variable loading has been realized. The following strength properties have been taken into calculation for stabilizer elements: Young's modulus $E=2.1x10^5$ Mpa, Poisson's ratio v=0.3.

Stresses state for the individual stabilizer elements has been calculated for different fixing configurations according to table 1 regarding to the number of bone screws and distance between a plate and a bone. Models have been loaded respectively: with the axial force 800N, with the bending moment 10Nm in a plate sagittal and frontal plane and with the torque moment 10Nm.

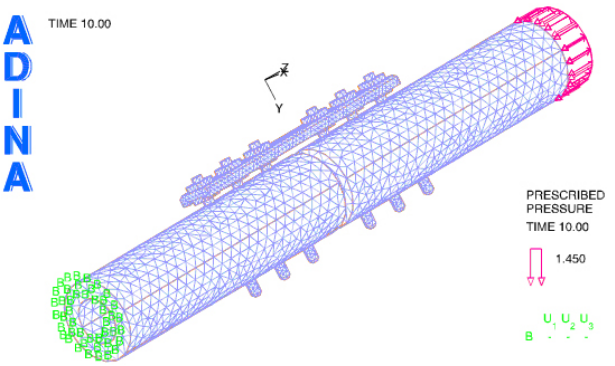

Fig. 3. Discrete model of the stabilizing system

Tab. 1. Designations of the analyzed fixing configurations.

Model	distance between plate and bone [mm]	number of screws
M 5-2	5	4 (2x2)
M 5-3	5	6 (2x3)
M 10-3	10	6 (2x3)
M 15-3	15	6 (2x3)

Finite Elements Method has been used for the calculations of stresses state in the stabilizer elements. The calculation has been performed with the ADINA system.

3. Results

Reduced stresses σ_{zr} distribution in the plate stabilizer elements in a M 5-3 model loaded with axial force 800N has been presented in fig. 4. Maximal stress value $\sigma_{zr\,max}$ = 390 [MPa] occurs on the central side of the bearing plate near the breaking gap.

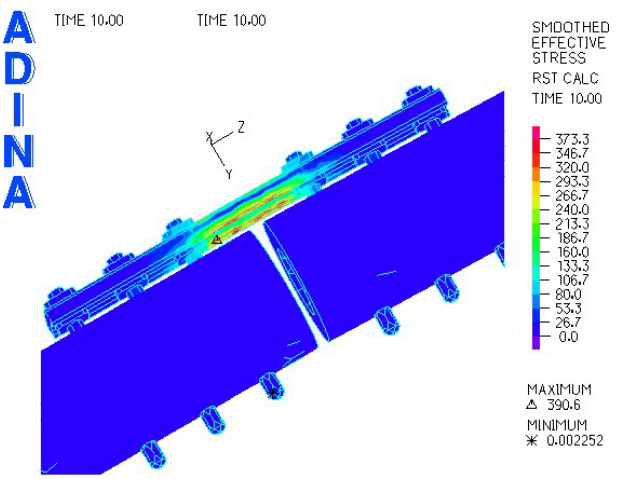

Fig. 4. Reduced stresses σ_{zr} [MPa] distribution in the plate stabilizer elements in a M 5-3 model loaded with axial force 800N.

Distribution of the normal stresses components towards z – σ_z presented in fig. 5 shows the form typical for bending

case. Extreme values of the σ_z stress occur on a surface of the stabilizer bearing plate and equal respectively to $\sigma_{z\,max}$ = 352 [MPa] and $\sigma_{z\,min}$ = – 411 [MPa].

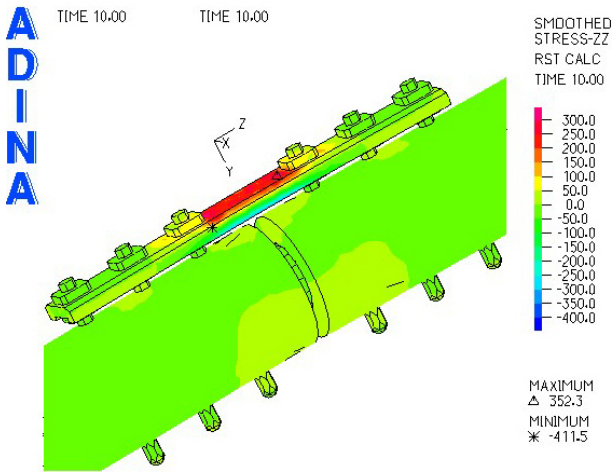

Fig. 5. Distribution of the normal stresses components towards z – σ_z [MPa] in the plate stabilizer elements in a M 5-3 model loaded with axial force 800N.

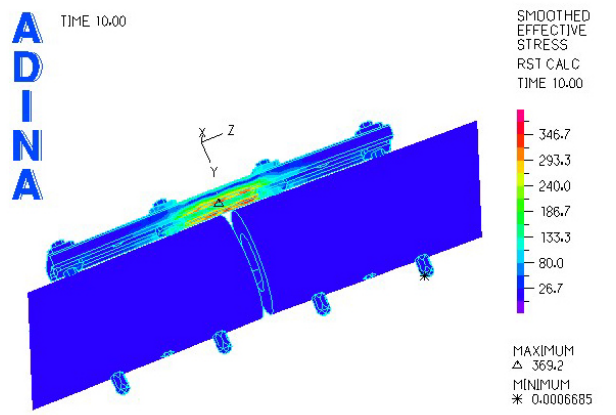

Fig. 6. Reduced stresses σ_{zr} distribution in the plate stabilizer elements in a M 5-2 model loaded with axial force 800N.

Increasing the distance between a plate and a bone has caused the significant increase in reduced stresses value to $\sigma_{zr\,max}$ = 470 [MPa] for a distance of 10 mm and $\sigma_{zr\,max}$ = 560 [MPa] for 15 mm (fig. 7).

Reduced stresses σ_{zr} distribution in the plate stabilizer elements in a M 5-3 model loaded with a 10 Nm bending moment in the sagittal plane (plate plane) has been presented in fig. 8. The maximal stresses values $\sigma_{zr\,max}$ =70 [MPa] occur along the lateral plate edges below the breaking gap.

Distribution of the normal stresses components towards z – σ_z in the plate stabilizer elements loaded with bending moment 10 Nm in the sagittal plane has been shown in fig. 9.

In a case of loading with a bending moment in the plate plane, movements of the bone fragments depend mainly from bone screws bending. It is visible in the increase in stresses values (M 15-3 model) in the central bone screws region where maximal reduced stresses occur under the bearing surface, and in the extreme screws where maximal values occur in the place where they nest into the bone (fig. 10).

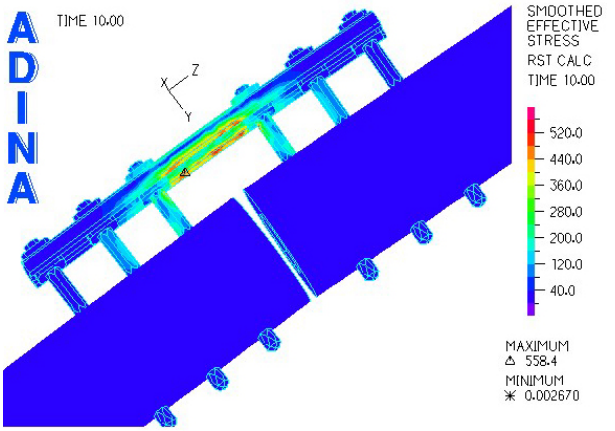

Fig. 7. Reduced stresses σ_{zr} [MPa] distribution in the plate stabilizer

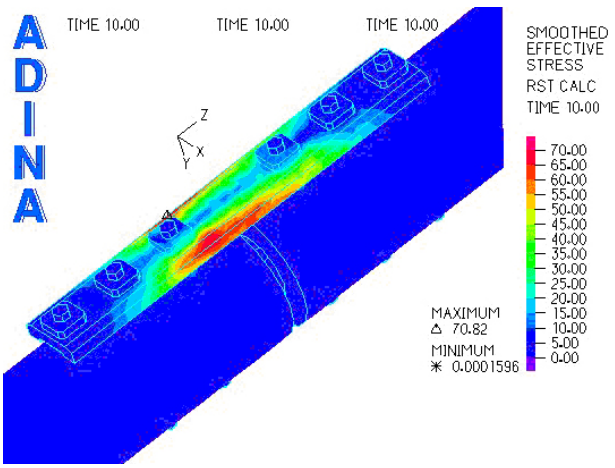

Fig. 8. Reduced stresses σ_{zr} [MPa] distribution in the plate stabilizer elements in a M 5-3 model loaded with bending moment 10 Nm in the plate plane.

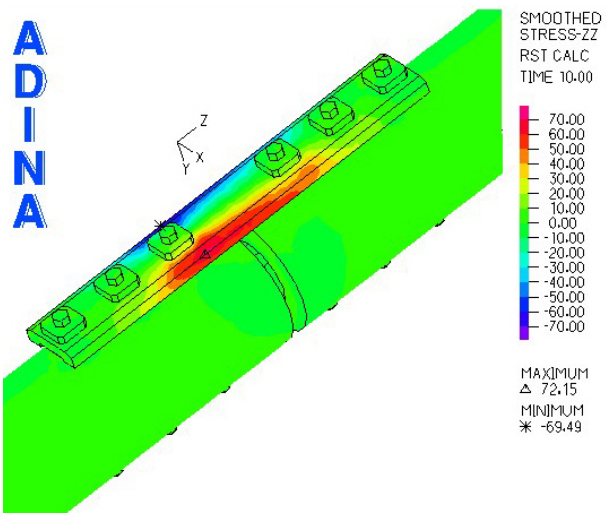

Fig. 9. Distribution of the normal stresses components towards z – σ_z [MPa] in the plate stabilizer elements loaded with bending moment 10 Nm in the sagittal plane.

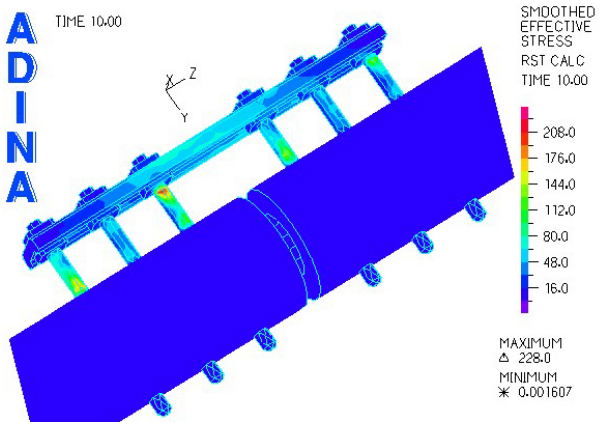

Fig. 10. Reduced stresses σ_{zr} [MPa] distribution in the plate stabilizer elements in a M 15-3 model loaded with bending moment 10 Nm in the plate plane.

In the bridging fixing loaded with bending moment 10 Nm in the frontal plane (symmetry plane) maximal stresses values $\sigma_{zr\,max}$ = 235 [MPa] similarly to the model loaded with axial force, occur in the lateral and central side of the plate near the central screw (fig. 11). Neither in a case of plate fixed with four screws nor for the change of distance between the plate and the bone the significant change in stresses distribution has been observed.

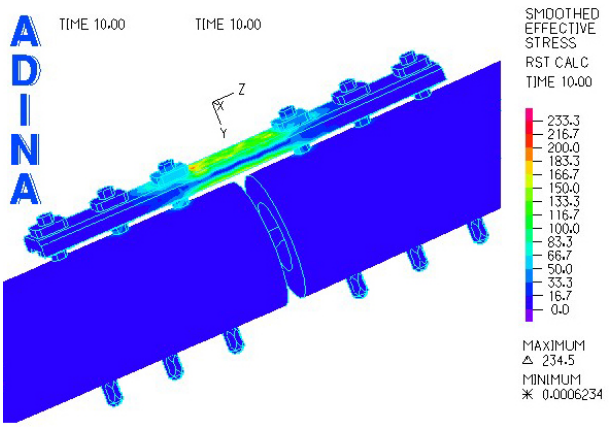

Fig. 11. Reduced stresses σ_{zr} [MPa] distribution in the plate stabilizer elements in a M 5-3 model loaded with bending moment 10 Nm in the longitudinal symmetry plane of the stabilizer.

Reduced stresses σ_{zr} distribution in elements of the plate stabilizer fixed 5 mm from the bone, in a bridging fixing model loaded with torque moment 10 Nm acting in the break plane has been presented in fig. 12. Maximal stresses $\sigma_{zr\,max}$ = 158 [MPa] occur un the region of central screw under the bearing surface

Fixing the stabilizer with four bone screws causes the increase in stresses value in central screws to 190 [MPa].

Increasing the distance between a plate and a bone results in significant increase of the reduced stresses in screws respectively to $\sigma_{zr\,max}$ = 280 [MPa] for a distance of 10 mm and $\sigma_{zr\,max}$ = 330 [MPa] for 15 mm (fig. 13).

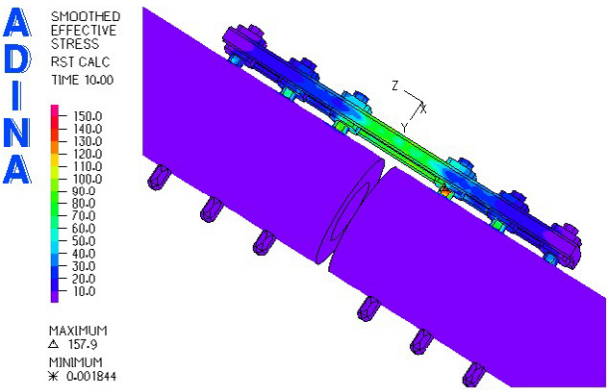

Fig. 12. Reduced stresses σ_{zr} [MPa] distribution in the plate stabilizer elements in a M 5-3 model loaded with torque moment 10 Nm.

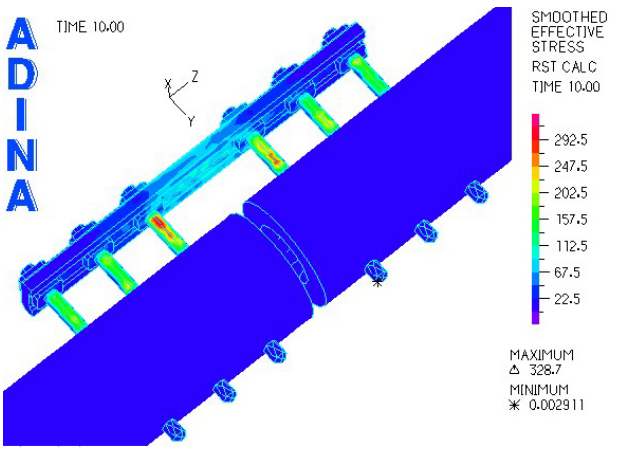

Fig. 13. Reduced stresses σ_{zr} [MPa] distribution in the plate stabilizer elements in a M 15-3 model loaded with torque moment 10 Nm.

4. Conclusions

Biomechanical tests of the plate stabilizer osteosynthesis confirm that, with a fixed geometry of the stabilizer bearing plate, elasticity of the fixing can be regulated by a appropriate number of bone screws and by a change of distance between plate and bone. Providing the specified mobility of the bone fragments is aimed towards creating the suitable conditions for forming the bone scar and for reconstruction into the bone.

Clinical observations show that the causes of most cases of trouble with bone adhesion are: incorrect implant selection, not considering the break biomechanics and improper implant installation.

The results of the calculations performed for a bridging fixing of ZESPOL plate stabilizer revealed that the stabilizer provides conditions for stable osteosynthesis in whole range of analyzed loading cases.

Obtained stresses distributions confirm the influence of the plate versus bone fixing as well as the mechanical loading in the change of stress state components in individual elements of the stabilize system.

Acceptable stresses values, leading to permanent deformation of the implant or its destruction, were not exceeded in any of the analyzed fixing models. However, unpredictable

increase in loading or cyclic change of loading can result in biomechanical insufficiency of the fixing system.

In a stabilizing model loaded with 800 N axial force the most loaded element is stabilizer bearing plate. Significant increase in stresses in the stabilizer bearing is observed with the distance of a plate from the bone. In a zone of the highest effort of the plate, on the level of break gap, reduced stresses amount to 560 [MPa] for maximal distance between plate and bone 15 mm.

In a case of loading of the system with torque moment and bending moment in a plate plane, the change of fixing the bearing versus bone leads to the stresses increase in bone screws.

Mobility of the bone fragments during loading of the bridging system with bending moment in a longitudinal symmetry plane of the plate, results mostly from the bending scale of the plate. Insignificant increase in bone fragments dislocation was observed with increasing the distance between plate and bone. Maximal reduced stresses values of 220 [MPa] were observed in a M 15-3 model in a stabilizer plate near the central screws.

Literature

1. Brudnicki J., Niedźwiedzki T.: Nieprawidłowości osteosyntezy jako przyczyna zaburzeń zrostu kostnego, Ortopedia Traumatologia Rehabilitacja, Volume 9, Number 3, s. 239-245, 2007.
2. Dudko S., Kusz D., Wojciechowski P., Nowak M.: Wybrane zagadnienia operacyjnego leczenia zaburzeń zrostu złamań trzonów kości długich, Chirurgia Narządów Ruchu i Ortopedia Polska, Tom 71, Z. 5, s. 353, 2006.
3. Granowski R., Sygnatowicz J.: Biomechaniczne podstawy osteosyntezy "ZESPOL", Biocybernetyka i inżynieria biomedyczna 2000, Tom 5, s. 519-541, Akademicka Oficyna Wydawnicza EXIT, Warszawa, 2004.
4. Gutier E., Perren S. M., Cordey J.: Effect of plate position relative to bending direction on the rigidity of a plate osteosynthesis. A theoretical analysis., Injury, 31, S-C 14-20, 2000.
5. Karnezis I. A., Miles A. W., Cunningham J. L., Lear month I. D.: ''Biological'' internal fixation of long bone fractures: a biomechanical study of a ''noncontact'' plate system, Injury, Vol. 29, No. 9, pp. 689-695, 1998.
6. Kusz D., Dudko S., Wojciechowski P., Guzik H.: Etiopatogeneza powikłań zrostu złamań trzonów kości długich, Chirurgia Narządów Ruchu i Ortopedia Polska, Tom 71, Z. 5, s. 344, 2007.
7. Marciniak J., Ramotowski W.: Osteosynteza stabilizatorami płytkowymi, Biocybernetyka i inżynieria biomedyczna 2000, Tom 5, s. 493-517, Akademicka Oficyna Wydawnicza EXIT, Warszawa, 2004.
8. Miclau T., Martin R.: The evolution of modern plate osteosynthesis, Injury, Vol. 28, No. 1. pp. S-A3-S-A6, 1997.
9. Ramotowski W.: Stabilizatory płytkowe Zespol i Polfix, Agencja Wyd. Zebra, Kraków, 1998.
10. Stoffel K., Dieter U., Stachowiak G., Gachter A., Kuster M. S.: Biomechanical testing of the LCP how can stability in locked internal fixators be controlled?, Injury Int. J. Care Injured, 34, S-B11 – SB19, 2003.

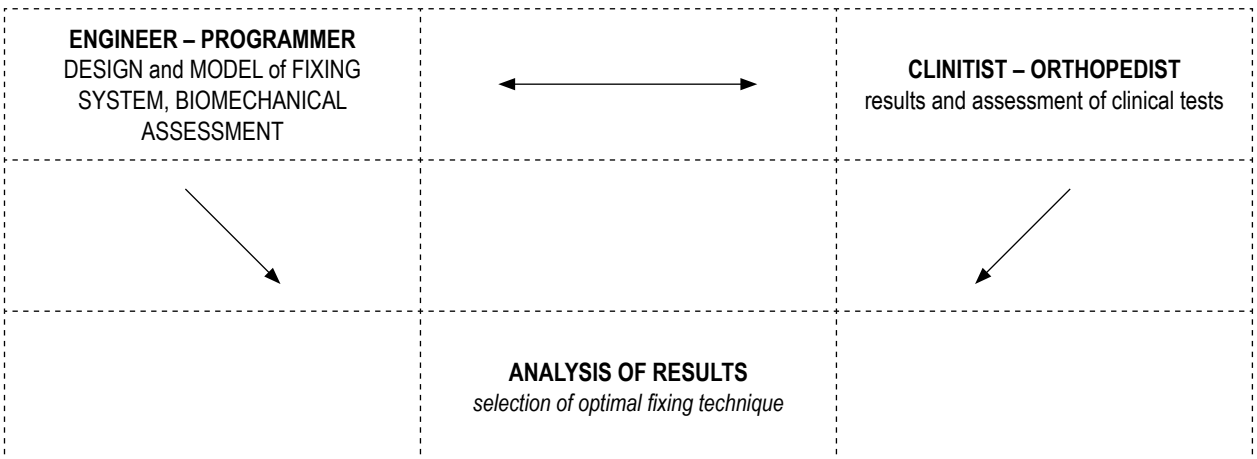

BIO-ALGORITHMS AND MED-SYSTEMS
JOURNAL EDITED BY MEDICAL COLLEGE – JAGIELLONIAN UNIVERSITY
Vol. 3, No. 6, 2007, pp. 37-39

MATHEMATICAL ONCOLOGY – WHAT IS IT ?

IRENA ROTERMAN-KONIECZNA

Department of Bioinformatics and Telemedicine – Collegium Medicum – Jagiellonian University, 31-530 Krakow, Lazarza 16, POLAND

Abstract: The large-size medical databases describe in details many medical phenomena including carcinogenesis in particular. The integrative analysis of the detailed information is highly expected nowadays. The development of interdisciplinary teaching is necessary to reach this goal. The construction of the algorithm simulating the all functions of organism (cell) is the aim of the proteomics. The properly (correctly) working proteom reconstructing processes in the cell when disturbed in aim-oriented form may produce as the result the system characteristic for particular disease. It is assumed to recognize in this way the processes leading to carcinogenesis in particular. This why even the new discipline is postulated: mathematical oncology linking the knowledge of medical problems with the ability of the applicability of mathematical methods.

Keywords: proteom, process simulation, cancerogenesis, bio-algorithm

Streszczenie: Rozwój technik analitycznych w medycynie spowodował znaczący wzrost rozmiarów baz danych szczegółowych dotyczących zjawisk medycznych w tym analiz procesów nowotworzeni w szczególności. Oczekuje się, że potrzebą chwili jest integracyjna analiza tych szczegółowych danych, która – jak się zakłada – może doprowadzić do systemowego modelu procesu kancerogenezy. W tym celu jednak istnieje pilna konieczność nauczania integracyjnego łączącego dyscypliny medyczne z naukami komputerowymi. Konstrukcja systemu algorytmicznego odwzorowującego funkcjonowanie organizmu żywego prowadząca do konstrukcji proteomu umożliwiłaby symulacje procesów świadomie zaburzonych. Uzyskanie zgodności rezultatów symulacji takiego układu z obserwacjami eksperymentalnymi, które nazywamy symptomami chorobowymi pozwoliłaby na uzyskanie systemowej odpowiedzi na pytania o źródła procesów chorobowych w tym nowotworzeni w szczególności. Do tego celu potrzeba jest interdyscyplinarnej edukacji. Postuluje się wręcz nauczanie onkologii matematycznej łączącej medycynę z matematyką.

Słowa kluczowe: proteom, symulacja procesu, nowotworzeni, bio-algorytm

XXI century is and certainly will be the century of information. The size of data bases is increasing so fast, that some problems of consuming them seem to rise the problems soon.

Biology seems to be an enormously large source of information as well as medical data particularly after sequencing the complete human genome and genomes of many other species.

Experimental oncology submits large sets of results. 21 000 of publications were registered in the year 2001. The diagnostics and therapy methods were described and reported there. The techniques to analyze the functioning of living organisms include the oncogenesis understood as change of structure and function of molecules responsible for biological activity controlling the living processes and death of healthy and pathological cells. About 200 genes have been identified in the human genome as enhancing and inhibiting the oncogenic processes.

Despite this abundance of information the mechanism of cancerogenic processes has not been recognized. The relations between processes are still unrecognized.

Oncology is desperately awaiting the models of qualitative as well as quantitative models allowing the consolidation and integration of sometimes very detailed and precise information. Data mining of the databases of such large size is possible only with the help of informatics.

On the other hand, the models recognized so far are too general to have the practical application. The degree of simplification introduced to model construction has been estimated as being too far to the medical practice. The clinicists, although they represent quite narrow specialization, are familiar with processes in details.

Each experiment can be characterized also as a very detailed one representing only a narrow fragment of the complete phenomenon. The clinicists, representing these narrow specializations, have difficulty to integrate their knowledge and to create the common model including all aspects representing medical specializations.

The papers oriented on biological aspects of processes in living organism are characterized as publications without any mathematical equation. The same can be said about scientific conferences. Clinical doctors and specialists in mathematics do not simultaneously participate in these conferences. The specialists in mathematics have no medical knowledge and the mechanism of biological processes is not recognized by them. On the other hand, mathematics is treated as a discipline distant versus the medical disciplines.

This distance seems to increase making the collaboration of these two specializations even more difficult.

The integration of the data collected in large databases and elaborating the common comprehensive language for these two disciplines seem to be of high importance nowadays. The medical studies do not expect of their candidates to be educated in mathematics as the discipline useful for the prospective profession. These phenomena have been made even more difficult limiting the mathematical education in high schools, particularly in the classes of biological orientation, where mathematics has been entirely eliminated. It is not a problem limited to one nation only. The same mistake has been made in many countries.

Very few specialists, acting in interdisciplinary areas finish their job after 'fitting the curve to the experimental points'. This procedure, which is important as the starting point, shall be developed to the possibly maximum extent leading even to the conclusion concerning the general mechanism. The important question in such a situation is: what kind of mechanism is responsible for the particular mathematical form? Maybe the specialists in mathematics resign too early without continuing the research as long as possible. The superficial analysis shall never satisfy the researcher without exploring the data until the general mechanism is discovered.

What actually shall be the main point for specialists in mathematical oncology ?

The best example to explain this idea is the discovery of colorectal carcinogenesis. The Authors of this success are Eric Fearon and Bert Vogelstein. Their idea was to link the genetics and epigenetics with the tissue morphology. In consequence, the complete mechanism has been presented explaining the mutual relations between normal mucosa, to small polyp to a large polyp and finally to invasive cancer.

The classic example is also the generation of cybernetics in 40-th of the XX century. The smart collaboration of the psychologist Ross Ashbi with the specialists in mathematics Norbert Wiener generated the origin of this new scientific specialization.

The models presented currently are usually not complete or not entirely correct. Their presence make clear that the next step is necessary to be done. This next step is strongly dependent on the preparation to interdisciplinary collaboration between specialists in medicine with specialists in mathematics. The main problem which must be solved is the elaboration of common language to make the communication possible. The way to reach this goal seems to be the description of commonly observed phenomena. This can be reached as a result of long lasting discussions which are not assumed to bring the results instantly. The time and patience seem to be critical.

The creation of the proteom – the complete set of proteins with the mutual relations between them - seems to be the first step to accomplish this goal. The construction of proteoms representing the entire organisms (bacteria, yeast or insects) particular organs. The main difficulty is to define the functional relation between proteins. The different criteria are accepted like activity in transport, gene expression etc or the relation of the hierarchy form. The mathematical models representing highly organized systems were tested and verified in electronics or economical processes. The models representing highly centralized systems (one decisive center) or dispersed (with a few decisive centers of equivalent power) and various forms of mixed models incorporating both systems (partially hierarchal, partially dispersed) have been presented and adopted to the biological systems.

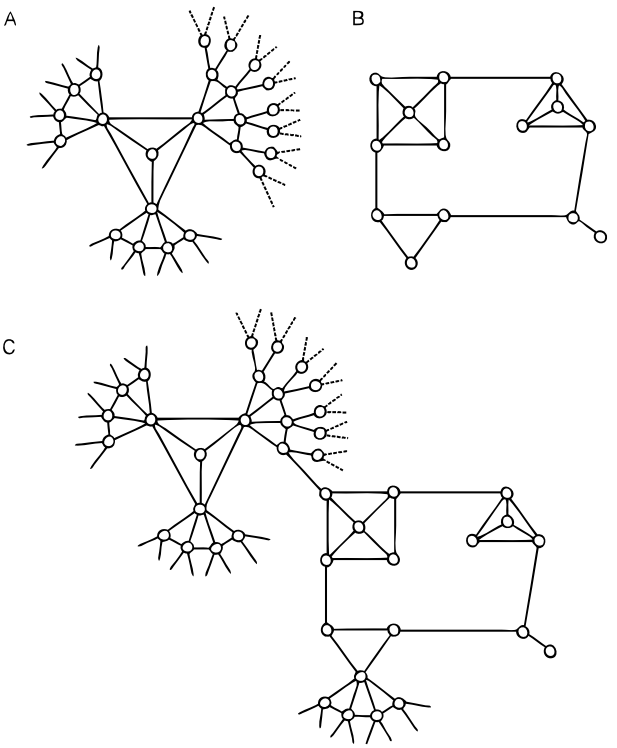

Fig.1. Simple presentation of different systems: A- hierarchal, B – dispersed, C – mixed (partially hierarchal, partially dispersed)

Proteoms have been constructed currently in spite of significant gaps on the list of proteins present in the cell (or organisms – in the human body about 1/3 of total number of proteins have not been recognized yet). The ideal solution which is the aim of the scientific activity is the repetition of the spectacular event in the science history, which is the Mendeleev's table.

Knowing only a part of the entire set of chemical elements the global system has been generated and even able to predict the chemical and physical characteristics of the missing elements.

The goal for all the scientists involved in the proteom generation is to form such a system which is able to put all the known proteins into their functional order and to localize the missing proteins in their correct points of the system.

The algorithm simulating the entire system with mutual relations between all the proteins representing particular biological functions may be the tool for enormously large number of simulation including pathological processes. The experiment of the category "*in silico*" for living organisms simulations could be available. The intentional damage of its elements may lead to the results which can be recognized as very well known diseases, the mechanism and origin of which is still unrecognized.

The sooner the collaboration between computer scientists and medical doctors starts the sooner the goal will be achieved. The comprehension and the interdisciplinary collaboration is necessary to reach this aim.

The initiation of interdisciplinary courses is necessary to make both the discussion and exchange of ideas possible. It seems to be the first necessary step toward the mathematical oncology initiation as the scientific specialization. The mathematical-natural studies have been continued since few years. It is pity that medicine does not appear as the discipline to be chosen for the students of mathematics. One may only hope that it will be available in a near future. The search for the enthusiasm for mathematics among the medical students as well as biological science oriented students of mathematics is quite difficult, although not useless. One of the main advantages of being the med-math or math-med specialist is a very cheep work place. All biological databases are available for free (Internet) and the computer equipment is quite cheep nowadays. The mathematical knowledge does not need large expenses. Databases are accessible by Internet (the unification of the large-scale information data concerning research on tumors is being introduced). It aims at consolidation of the effects of many centers in such a way that the data coming from various laboratories could be available for analysis

The access to internet and cheep PC together with freely available medical databases seem to be enough to make the dream of the hardest disease – cancer – to be recognized and successfully treated.

The text presented was based on the publications given in references.

References

1. Gatenby R.A., Maini P.K. (2003) Cancer summed up. *Nature,* 421, 321.
2. Fearon E.R., Vogelstein B.A. (1990) A genetic model for colorectal tumorigenesis. *Cell*., 61 (5), 759-67.
3. Taylor W.R. (2002) A 'periodic table' for proteins. *Nature*, 416, 657-660.
4. Gavin A.-C., Bösche M., Krause R., Grandi P., Marzioch M., Bauer A., Schultz J., Rick J., Michon A.-M., Cruciat C.-M., Remor M., Höfert C., Schelde M., Brajenovic M., Ruffner H., Merino A., Klein K., Hudak M., Dickson D., Rudi T., Gnau V., Bauch A., Bastuck S., Huhse B., Leutwein C., Heurtier M.-A., Vopley R., Edelman A., Querfurth E., Rybin V., Drewes G., Raida M., Bouwmeester T., Bork P., Seraphin B., Kuster B., Neubauer G., Superti-Furga G. (2002) Functional organization of the yeast proteome by systematic analysis of protein complexes. *Nature*, 415, 141-147.
5. Koonin E. V., Wolf Y. I., Karev G. P. (2003) The structure of the protein universe and genome evolution. *Nature*, 420, 218-223.
6. Eigen M., Schuster P. (1979) The hypercycles – A principle of natural self-organization. Springer Verlag – Berlin, Heidelberg, New York.
7. Shannon C. E. A. (1948) Mathematical theory of communication. *Bell Syst Tech J*, 27, 379-423.

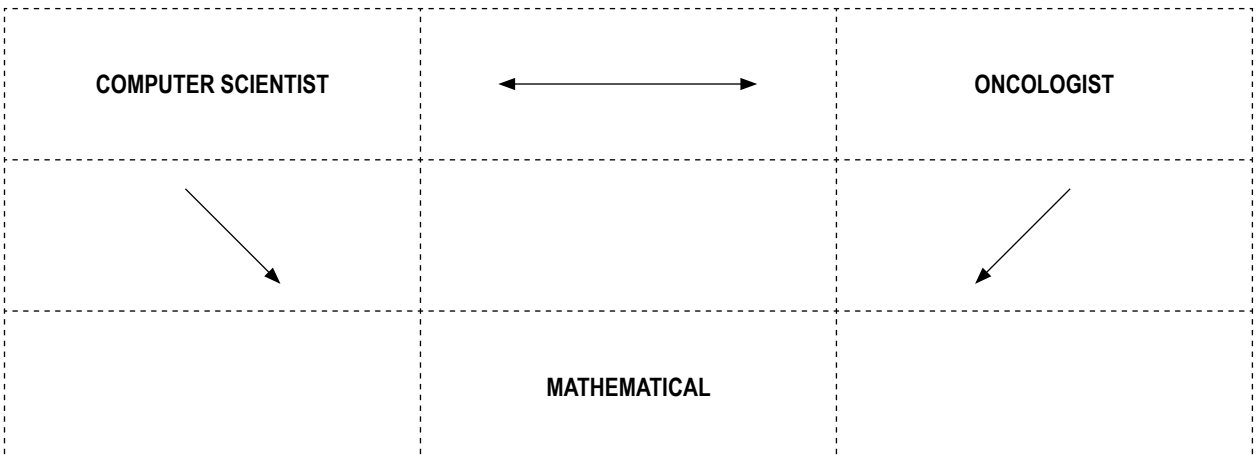

BIO-ALGORITHMS AND MED-SYSTEMS
JOURNAL EDITED BY MEDICAL COLLEGE – JAGIELLONIAN UNIVERSITY
Vol. 3, No. 6, 2007, pp. 41-44

THE NATIONAL PAEDIATRIC DIABETES REGISTRY: AN ELECTRONIC DATABASE SYSTEM AIMED AT OPTIMIZATION OF PAEDIATRIC DIABETES MANAGEMENT IN POLAND

Łukasz Walenciak[1], Przemysław Pierściński[1], Wojciech Fendler[1],
Agnieszka Szadkowska[1,2], Wojciech Młynarski[1,2]

[1] Departement of Paediatrics Medical Univeristy of Lodz
[2] The 4th Clinical Hospital of Medical Univeristy of Lodz
Sporna 36/50, 91-738 Lodz, Poland, Phone 48 42 617 77 69, Fax 48 42 617 77 72

Abstract: Treatment of a diabetic paediatric patient is a complex issue, requiring adherence to current medical standards and adjusting of goals and methods of treatment to patient's capabilities. The number of paediatric patients with diabetes is constantly growing, and in the year 2009 is estimated to exceed 10.000 nationwide. In order to provide them with appropriate care, and at the same time, to observe epidemiologic trends and determine causative factors of this disease, a tool providing means of data collection and analysis is ubiquitous. National Paediatric Diabetes Registry (NPDR) is a project aiming to improve and unify data flow of diabetic patients in developmental age. The project is also expected to raise the standards of medical treatment by preparing regular staff trainings and monitoring treatment results in all participating diabetic paediatric centres in Poland.
Goals of the project will be achieved through the use of computer infrastructure for managing patient's data, his/her medical examinations and observing the course of treatment. The software created for this purpose uses the technology and architecture of distributed databases controlled by a central system responsible for the logical coherency of the physically dispersed database fragments. Applications in diabetic clinics serve as local databases for the purpose of everyday practice and as sources of anonymous medical data for the central database.
The system will be able to collect vast amount of diverse data enabling easy and effective analysis of the courses of treatments of both, individual patient and cross-sectional epidemic data. Simultaneously, it will allow us to pinpoint centres with therapeutic results below expectations, and identify the cause of this situation. The program will also serve as major screening tool in search for special types of diabetes such as MODY or neonatal diabetes. These patients could be considered to follow different, pharmacogenetic treatment methods, improving their metabolic control and quality of life.
Introducing the unified system of diabetic children care will also streamline the cooperation and exchange of data between Clinics participating in the Program, thus ensuring appropriate level of care and its maximum availability, regardless of location in which a particular patient is treated.

Keywords: Children, metabolic disorders, register, diabetess

Streszczenie: Leczenie młodego pacjenta z cukrzycą jest skomplikowanym procesem, wymagającym stosowania się do aktualnych standardów medycznych oraz dopasowywania metod oraz celów leczenia do możliwości pacjenta. Liczba pacjentów pediatrycznych z cukrzycą stale rośnie i przewiduje się, iż w roku 2009 przekroczy ona ilość 10.000 w skali kraju. W celu zapewnienia im należytej opieki i, równocześnie, obserwowania trendów epidemiologicznych oraz wyznaczenia przyczyn tej choroby, niezbędne jest narzędzie do gromadzenia i analizy danych. Krajowy Rejestr Cukrzycy Wieku Rozwojowego jest projektem mającym na celu usprawnienie oraz zunifikowanie przepływu danych o pacjentach w wieku rozwojowym z cukrzycą. Oczekuje się, że projekt ten podniesie także standardy opieki medycznej poprzez cykle szkoleń oraz obserwację wyników leczenia we wszystkich pediatrycznych klinikach diabetologicznych w Polsce zaangażowanych w realizację tego przedsięwzięcia.
Cele te zostaną osiągnięte poprzez zastosowanie infrastruktury komputerowej do zarządzania danymi pacjenta, jego badaniami oraz obserwowania przebiegu całego leczenia. Stworzone do tego celu oprogramowani,e korzysta z technologii i architektury rozproszonych baz danych, będących pod kontrolą centralnego systemu odpowiedzialnego za logiczną spójność rozproszonych fizycznie baz danych. Aplikacje w klinikach diabetologicznych pełnią rolę lokalnych baz danych dla celów codziennej pracy kliniki oraz jako źródła anonimowych danych medycznych dla bazy centralnej. System będzie w stanie zebrać szeroka gamę różnorodnych danych umożliwiając łatwą oraz efektywną analizę przebiegów leczenia dla obydwu rodzajów danych, indywidualnych danego pacjenta oraz epidemiologicznych. Jednocześnie, pozwoli to na dokładne zlokalizowanie klinik z wynikami terapeutycznymi poniżej oczekiwań oraz zidentyfikować powody takich sytuacji. Program ten będzie także służył jako główne narzędzie badawcze do poszukiwań nietypowych typów cukrzycy, takich jak MODY czy cukrzyca noworodkowa. Tacy pacjenci mogliby być wtedy poddani innym, farmakogenetycznym metodom leczenia, polepszającym kontrolę metaboliczną ich choroby oraz jakość życia.
Wprowadzenie ujednoliconego systemu dziecięcej opieki diabetologicznej uprości dodatkowo współpracę oraz wymianę danych pomiędzy klinikami uczestniczącymi w programie, a co za tym idzie poziom opieki medycznej i jej dostępność niezależnie od miejsca zamieszkania pacjenta.

Słowa kluczowe: dzieci, choroby metaboliczne, rejestr, cukrzyca

1. Introduction

Recent epidemiology studies have shown a dramatic worldwide increase in the prevalence of diabetes. This also affects population of children and adolescents [1-4]. Moreover, the structural changes among the diabetic population have also been noted, e.g. an increase in frequency of type 2 diabetes among paediatric patients [5-6]. These changes were the motive force to establish nationwide registries of paediatric diabetes in many countries, including Poland [7-9].

As opposed to the situation common with adult diabetic patients, children are treated almost exclusively in academic medical units. However, paediatricians strive to achieve more stringent therapeutic goals for their patients, than is the case with adults. The exact course of treatment may be individualized and is associated with local standards and peculiarities of entire unit, individual experience of the physician and his or her experience in the field of diabetes, paediatrics and psychology. This range of influence makes the exchange of data between such facilities difficult and seemingly unnecessary, as all units may deem themselves as autonomic and self-sufficient. Such a model however, creates problems in collection of epidemiological data. At present, collecting credible information on the subject is very difficult. Comparison of metabolic control and treatment goals is easier, as all units adhere to international and national guidelines, although data exchange is based only on individual cooperation and good-will of physicians. Since there are differences in patients education and intensity of diabetes therapy among paediatric centres there is a distinct need for improvement of this situation.

On the other hand, such a dispersed system creates the possibility of developing local standard of treatment and further improvement in diabetes management among paediatric and adolescent patients. Additionally, a small number of such units allows for the possibility of connecting them together in a form of a dispersed network enabling data exchange. Such approach is feasible only in the paediatric, but not adult diabetes management in Poland.

The aim of this project is to design and develop a distributed database system for the purpose of better organization of paediatric diabetes treatment as well as collection and analysis of medical data. This, in turn, will provide optimum standardisation of treatment procedures, provide physicians with accurate epidemiologic tools and possibly contribute to the identification of patients with unusual types of diabetes and finally.

2. System design

The overall concept of the entire system is to enable physically distant diabetic centres to be a part of a centralised 'diabetic network'. All participants, the central unit and diabetic clinics, while cooperating with each other, will preserve their ability to work independently.

A general graph of the project's organization structure is presented below (Figure 1).

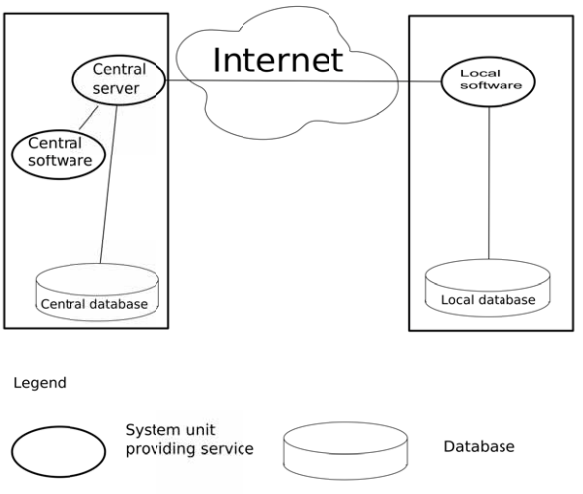

Fig. 1. Overall system design

Technology

In choosing the optimum technology, the areas most emphasised were: data security, efficiency and time- and cost-effectiveness development. Additionally, specific target software and hardware environment also played a crucial role in this choice. The software will not be publicly accessible. The only type of users, will be physicians involved in diabetologic care. As this group is a highly qualified society with high expectations concerning software usability and characterized by different work experience with particular programmes, the clinic application will have to be properly adjusted to suit their needs and expectations.

The entire system on both end nodes (central and client) was planned on the foundation of .NET 2.0 platform. The .NET 2.0 Framework is a software component that supports building and running of modern applications [10]. It has been designed to provide a code execution environment minimising software deployment effort and promoting safe execution of the code. It has powerful set of libraries and modules like Common Type System allowing the developer to benefit from the language independence, simplified project deployment and security trust level code execution [10-11].

The main implication of this choice, is the choice to use SQL Server 2005 as the database providing excellent system efficiency and reliability in this registry. SQL Server is a relational database management system [12]. It is produced in several versions to meet the needs and expectations of the variety of users and their requirements [13]. As the discussed project benefits from the use of free Express edition in the clinics and Standard edition, powerful data handling centre, in the project central, SQL Server 2005 also features automated database mirroring, failover clustering, and database snapshots, functions that will be used in the central database design and development [13-14]. The secure by design policy also sets the proper default level of data security on the client, clinic, side minimising the risk of the IT specialist to be called upon to deploy it [14].

2.2. Functionality

2.2.1. Client side

The diabetologic clinic is responsible for gathering patient data, required in the process of treatment. Such data is henceforth used as a patient medical chart in an electronic environment. Clinics update their databases regularly, depending on the patients' visit schedules. At this stage, no significant changes will take place in the routine day-to-day running of the clinics and storage of information about patient. The only alteration is the standardised computerisation of the process.

It is of crucial importance, that only authorised personnel will be able to access the client application. Each registered user has to log in to the software with a unique pair of login and password. Only after positive verification it will be possible to work on the patient data stored at a particular site. It is not possible to view other clinic's patient database via the central system.

The Client application is responsible of accepting all the data that is related to the patient course of treatment. This data is carefully validated before reaching even the local, clinic database, to ensure the proper data values as well as types. A great effort is made to allow the most flexibility possible is this situation as no designer is able to predict all test cases. Strict validation is essential to maintain database coherency and significance of information stored in the database along with meaningful relations.

Besides the most basic operations like adding a new patient and subsequently his or her regular visits, client application is responsible for generating various reports and summaries. Those range from official reports for the National Health Fund to various local summaries improving, for example, analysis of the current course of treatment of the specific patient. An example of user interface in client application is presented below (Figure 2).

2.2.2. Central side

Via the Internet clinics send their anonymous patients data to the central database responsible for storing the incoming data. At the central side of the system there is a set of tools enabling thorough analysis, performing data mining operations, but also acts as a backup copy of the patients data. It is also worth noticing that the central does not need to know the whereabouts of the clinics as it is the clinics that initiate the connection knowing where the central is located in the Internet.

Central node of the system is the place of storage of all the data gathered in clinics. Here, various treatment results can be easily statistically checked being already validated and entered in a suitable database system. Based on those analysis and their findings there is possibility of further examinations of the material in the laboratory of the central unit. Results will be also available in the application of the specific clinic.

2.3. Implementation

The backbone of the system is the distributed databases architecture. Distributed databases systems are the combination of two branches of computer science: database systems and computer networks. More formal definition defines such technology as a collection of multiple, logically interrelated databases distributed over a computer network [15]. The model used, resembles the client/server model with the clinics being the clients and the central database being the server [15].

With such architecture, one of the crucial issues concerning the success of the system is the security of the sensitive data being transferred over the Internet. The design uses the cryptographic protocols (TLS 1.1). Additionally the uncertain nature of Internet connections enforces the strong use of transactions. The crucial issue in this matter is to ensure completeness of

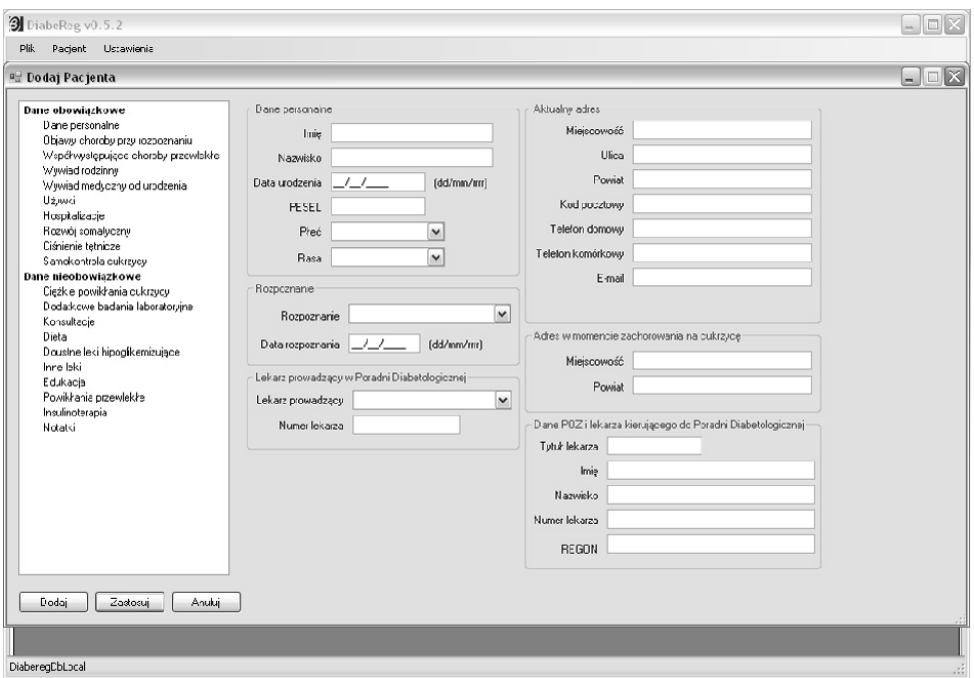

Fig. 2. Example of interface in clinic application

enormous amounts of data being sent. The transactions must be either complete or not performed at all. Therefore, all databases will remain coherent and synchronised, which is a key requirement for implementation of a distributed database system. Interrupted actions will not be registered in the main database and the entire operation will be postponed and performed again at the next opportunity.

3. Discussion

Devising a project of this magnitude requires meticulous planning, designing and implementation. The overall system will be complex, multi-tiered and distributed cooperation between applications, databases, operating software and hardware. As with any project, each has to begin at some stage, only to be constantly expanded during the development timeline. The implementation plan assumes the creation of local, client software and expanding it and providing additional functionality. This project described the initial steps in the process of creating a nationwide registry.

However, even with the fully operational system there is no guarantee of the project success. To ensure a positive effect of the registry, the system has to be used by the clinics' staff, who will be motivated to see benefits of joining to the program. This will require changes in the already established medical environment and local data and patient handling habits. The extra effort will have to be made outside the scope of the project implementation, to convince future users to participate in the NPDR. Such attempts were already organized on several paediatric and diabetic conferences, where the demonstration version of the software was shown and discussed. Physicians witnessing those presentations showed interest in the project and its outcomes and anticipate the implementation stage.

In conclusion, the project is a great chance to improve the level of diabetic care in children and adolescents with diabetes. The authors expect the first benefits to manifest shortly after full implementation to all clinical centres as an comprehensive epidemiologic analysis of data will be prepared by the central. The outcomes are hard to predict, however it will surely benefit the entire paediatric society dealing with diabetes and provide paediatricians with valuable insight and motivation to educate their patients and adjust therapeutic and educational methods to allow their patients to reach the best national results of metabolic control of diabetes.

Acknowledgments

This project has financial support from the Polish Ministry of Health from the to the Program for Prevention and Treatment of Diabetes in 2006-2008.

References

1. Green A.: The EURODIAB studies on childhood diabetes 1988-1999. Europe and Diabetes. *Diabetologia* 44 Suppl 3:B1-B2, 2001.
2. Szadkowska A., Czerniawska E., Bodalski J.: Zapadalność na cukrzycę typu 1 wśród dzieci i młodzieży regionu łódzkiego w latach 1983-2000. *Prz Pediatr* 33: 2003.
3. Jarosz-Chobot P., KBO-BE: Increasing trend of incidence of diabetes mellitus type 1 in children aged to 15 yrs in Upper Silesia region (Poland) in 1989-2000. *Diabetologia* 45 Suppl 2:A 62, 2002.
4. Kretowski A., Kowalska I., Peczynska J., Urban M., Green A., Kinalska I.: The large increase in incidence of Type I diabetes mellitus in Poland. *Diabetologia* 44 Suppl 3:B-8-B50, 2001.
5. Rosenbloom A.L.: Increasing incidence of type 2 diabetes in children and adolescents: treatment considerations. *Paediatr Drugs* 4:209-221, 2002.
6. Duncan G.E.: Prevalence of diabetes and impaired fasting glucose levels among US adolescents: National Health and Nutrition Examination Survey, 1999-2002. *Arch Pediatr Adolesc Med* 160:523-528, 2006.
7. Tuomilehto J., Karvonen M., Pitkaniemi J., Virtala E., Kohtamaki K., Toivanen L., Tuomilehto-Wolf E.: Record-high incidence of Type I (insulin-dependent) diabetes mellitus in Finnish children. The Finnish Childhood Type I Diabetes Registry Group. *Diabetologia* 42:655-660, 1999.
8. Olsen B.S., Svensson J., Mortensen H.B.: The Danish registry for child and adolescent diabetes. The Danish Society of Child and Adolescent Diabetes. *Ugeskr Laeger* 168:1210, 2006.
9. Bodalski J., Szadkowska A., Młynarski W.: Ogólnopolski Rejestr Cukrzycy Wieku Rozwojowego – nadzieje i oczekiwanie. *Przegl. Ped.* 36(3):175-180, 2006.
10. Microsoft MSDN Library: .NET Framework Conceptual Overview [online] <http://msdn2.microsoft.com/en-us/library/zw4w595w(VS.80).aspx>, 2008.
11. Microsoft MSDN Library: Overview of the .NET Framework [online] <http://msdn2.microsoft.com/en-us/library/a4t23ktk(VS.80).aspx>, 2008.
12. Microsoft Corporation: SQL Server 2005 Platforma zarządzania i analizy danych – Opis funkcjonalny, 2005.
13. Microsoft Corporation: Porównanie funkcji SQL Server 2005 [online] <http://www.microsoft.com/poland/sql/prodinfo/compare/default.mspx>, 2008.
14. Microsoft MSDN Library: SQL Server 2005 Documentation [online] <http://msdn2.microsoft.com/en-us/library/ms203721.aspx>, 2008.
15. Ozsu M.T., Valdurez P.: Principles of Distributed Database Systems. Second edition. London: Perentice-Hall, Inc., 1999.

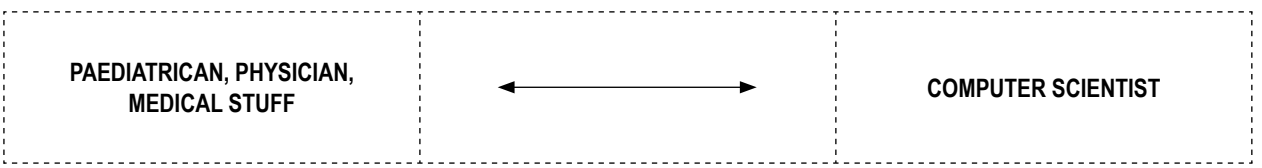

BIO-ALGORITHMS AND MED-SYSTEMS
JOURNAL EDITED BY MEDICAL COLLEGE – JAGIELLONIAN UNIVERSITY
Vol. 3, No. 6, 2007, pp. 45-51

QUALITY OF LIFE OF PATIENTS WITH INFLAMMATORY BOWEL DISEASE

Anna Wysopal, Magdalena Przybylska

Chair of Gastroenterology, Hepatology and Infectious Diseases
Collegium Medicum – Jagiellonian University – Kraków Poland

Abstract: Inflammatory bowel disease (IBD) is a group of illnesses that are characterized by inflammation of the intestine: ulcerative colitis (UC), Leśniowski-Crohn's disease (CD), and unspecified forms (with features characteristic for both CD and UC). Inflammatory bowel disease is a chronic disorder characterized by periods of remission and unpredictable relapses. Like each chronic disorder it has impact on quality of life.
Te aim of our study was to assess how much the disease decreases the quality of life and to consider how it can be improved.
Sixty nine patients IBD patients treated in Department of Gastroenterology, Hepatology and Contagious Diseases of Jagiellonian University Medical College were enrolled in the study. The patients completed a questionnaire (SF-36). Their scores were compared with those of general population. IBD patients' quality of life was impaired in physical as well as psychological aspects. The main conclusion is that patient beside internal consultation should include regular psychological counseling. This should improve the psychological aspect of life of IBD patients and decrease frequency of exacerbations.

Key words: IBD, UC, quality of life

Streszczenie: Nieswoiste zapalenia jelit (IBD) to grupa chorób, których istotą jest proces zapalny toczący się w ścianie jelita. Obejmuje ona takie jednostki jak: wrzodziejące zapalenie jelita grubego (UC), chorobę Leśniowskiego-Crohna (CD) i postaci nieokreślone (cechy charakterystyczne zarówno dla CD jak i UC). Nieswoiste zapalenia jelit to przewlekłe choroby charakteryzujące się okresami remisji i nieprzewidzianych zaostrzeń. Jak każda przewlekła choroba, IBD wpływa na jakość życia.
Celem naszych badań było określenie w jakim stopniu choroba obniża jakość życia oraz zastanowienie się jak można ją polepszyć.
Sześćdziesięciu dziewięciu pacjentów leczonych w Klinice Gastroenterologii, Hepatologii i Chorób Zakaźnych Collegium Medicum Uniwersytetu Jagiellońskiego zostało włączonych do badania. Pacjenci uzupełniali kwestionariusz (SF-36). Wyniki które uzyskali zostały porównane z wynikami grupy kontrolnej. Główny wniosek: pacjenci prócz konsultacji internistycznej powinni mieć dostęp do regularnych konsultacji z psychologiem. To powinno polepszyć psychologiczny aspekt życia pacjentów z IBD i w konsekwencji zmniejszyć częstość zaostrzeń.

Słowa kluczowe: IBD, UC, jakość życia

Background

Inflammatory bowel disease (IBD) refers to chronic diseases that are characterized by inflammation of the intestine: ulcerative colitis (UC), Leśniowski-Crohn's disease (CD) and unspecified forms (with features characteristic for both CD and UC). The most common symptoms include abdominal pain varying in localization and intensity, cramping, diarrhea, bloody stools, nausea, vomiting and in the course of IBD bleeding from the gastrointestinal tract. Some patients have extra-intestinal manifestations of IBD. Virtually any organ may be affected, but most commonly these involve joints, the skin, liver, bile duct, vascular and eye problems.

IBD is a chronic disorder characterized by periods of remission and unpredictable relapses. The first flare-up can commence at any age, but their highest incidence occurs between 15 and 40 years of age [1]. They have a great impact during a very active period of life that often includes acquiring education, developing a carrier and raising a family [2]. Pharmacotherapy carried for years allows for long term remissions. Many patients are able to lead a normal life due to such treatment. However, a lot of patients have an impaired quality of life with physical, social, and emotional dysfunctions.

The aim of our study was to assess the degree of the quality of life decrease and to consider how it can be improved.

Methods

Eighty-five IBD patients of Department of Gastroenterology, Hepatology and Contagious Diseases of Jagiellonian University Medical College were enrolled in the study during a period of remission.

All the patients had clinically diagnosed and histopathologically confirmed IBD. All the patients were asked to complete a questionnaire. It has been proved in several studies that disease activity has a great impact on quality of life [3], thus only patients in remission were included in the study.

At first population study included 69 patients (81.8%) with UC, and 16 patients (18.2%) with Leśniowski-Crohn's disease.

Due to small number patients with Leśniowski-Crohn disease, this group was excluded from the study. As a result, the population study included 39 women (56.5%) and 30 men (43.5%) with UC.

Additionally, a control group was selected. Lack of chronic disease(s) was the essential condition for inclusion into the control group. The control group included 74 people: 43 women (58.1%) and 31 men (49.1%).

The mean age in these two groups was 37.6+/-14,3 range from 20 to 90.

To assess the quality of life the Short Form 36 Health Survey (SF-36) was used. The SF-36 is a widely used generic instrument. It consists of 36 questions grouped into eight dimensions. The access of the Jagiellonian University Medical College to SF-36 is licensed.

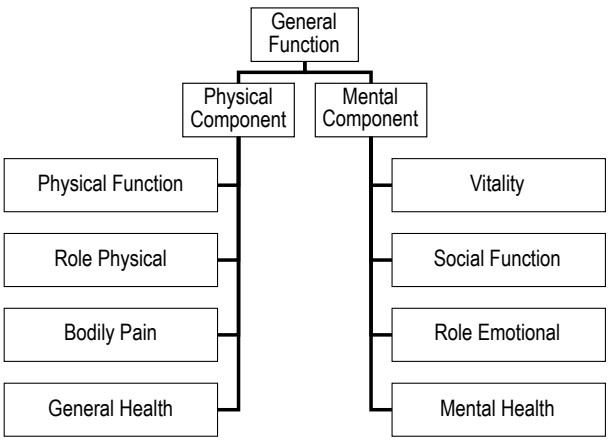

Fig 1. SF-36 Scales Measure Physical and Mental Components of Health

Statistical Analysis

Descriptive statistics are reported as mean, standard deviation (SD), median and range. Comparable analysis was performed using t-Students test. Mann-Whitney test was used for variables representing other than normal distribution. The influence of age on IBD patient's quality of life was assessed using correlation analysis: correlation coefficient (r) .

Results

The statistical significance was recognized for $p<<\alpha$ for $\alpha=0.05$.

Physical Function-mean score for the patients with UC was 76 points and it was significantly lower in comparison to the control group. The activities such as: getting dressed, shopping, house cleaning were included in this dimension. The lower points showed that UC patients had more difficulty with daily activities.

Problems with work and other daily activities were related to difficulties in physical function. Thus, there is nothing surprising that the patients with IBD had a much lower mean score for this dimension (UC-43 points, background population-82 points)

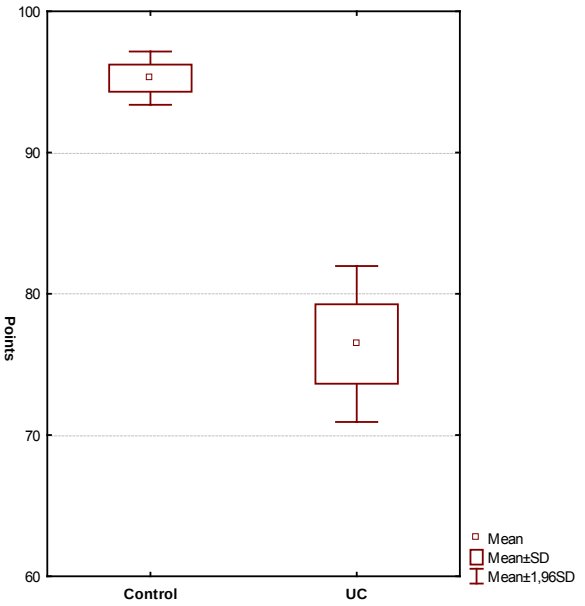

Fig. 2. Physical Function-comparison between the control group and UC patients

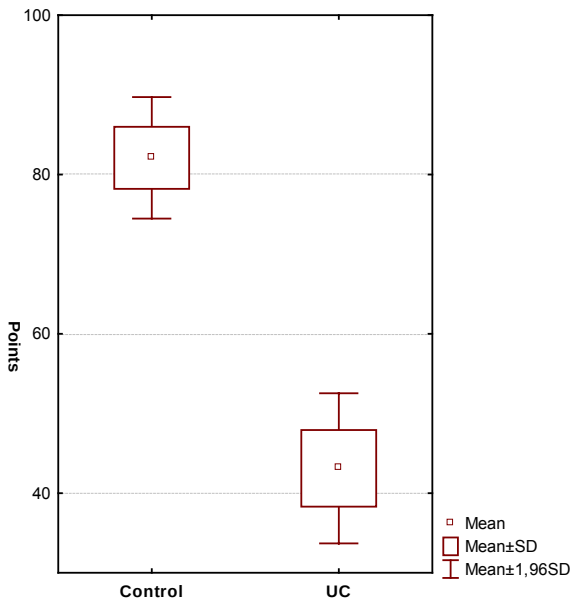

Fig. 3. Role Physical-comparison between the control group and UC patients

Table 1. Criteria included in SF-36 questionnaire. Each of the dimension scores is expressed as a value between 0 and 100 with higher scores representing better health [4].

Dimension	Abbreviation	Definition	Items
Physical Functioning	PF	Limitation in performing daily activities	3a-3j
Role Physical	RP	Problems with work and other daily activities as a result of physical health	4a-4j
Bodily Pain	BP	Intensity of pain and limitation due to pain	7-8
General Health	GH	Evaluates personal pain	1,11a-11d
Vitality	V	Frequency of feeling worn out / full of energy	9a,9e,9g,9i
Social Functioning	ScoF	Limitation in social activities due to physical and emotional problems	6,10
Role Emotional	ER	Problems with work or other activities as a result of emotional problems	5a-5c
Mental Health	MH	Feelings of nervousness and depression	9a,9c,9d,9f,9h
		First 4 criteria-general physical function Second 4 criteria- general mental function	

Table 2. Assessment of differences between the UC patients and control group.
PF-Physical Functioning, RP-Role Physical, BP-Bodily Pain, GH-General Health, PCS-Physical Summary Component V-Vitality, ScoF-Social Functioning, ER-Role Emotional MH-Mental Health, MCS-Mental Summary Component

Dimension	Groups	mean	SD	median	min	max	value p
PF	UC	76.45	23.39	80.00	0.00	100.00	0.0001
	Control	95.27	8.27	100.00	70.00	100.00	
RP	UC	43.12	39.96	50.00	0.00	100.00	0.0001
	Control	82.09	33.50	100.00	0.00	100.00	
BP	UC	56.25	26.49	52.00	0.00	100.00	0.0001
	Control	78,84	21.14	84.00	22.00	100.00	
GH	UC	43.71	23.05	40.00	0.00	100.00	0.0001
	Control	72.91	18.05	77.00	22.00	100.00	
PCS	UC	54.88	23.00	55.50	6.75	100.00	0.0001
	Control	82.28	15.96	87.25	37.25	100.00	

Dimension	Groups	mean	SD	median	min	max	value p
V	UC	44.93	21.08	50.00	0.00	90.00	0.0001
	Control	60.88	16.25	60.00	20.00	95.00	
Socf	UC	55.98	26.74	50.00	0.00	100.00	0.0001
	Control	78.72	18.36	75.00	25.00	100.00	
ER	UC	55.07	41.15	33.33	0.00	100.00	0.0100
	Control	72.97	40.42	100.00	0.00	100.00	
MH	UC	54.20	19.41	56.00	12.00	88.00	0.0050
	Control	62.76	16.43	64.00	20.00	92.00	
MCS	UC	52.55	23.48	50.83	9.25	93.25	0.0001
	Control	68.83	18.47	71.56	21.38	96.75	

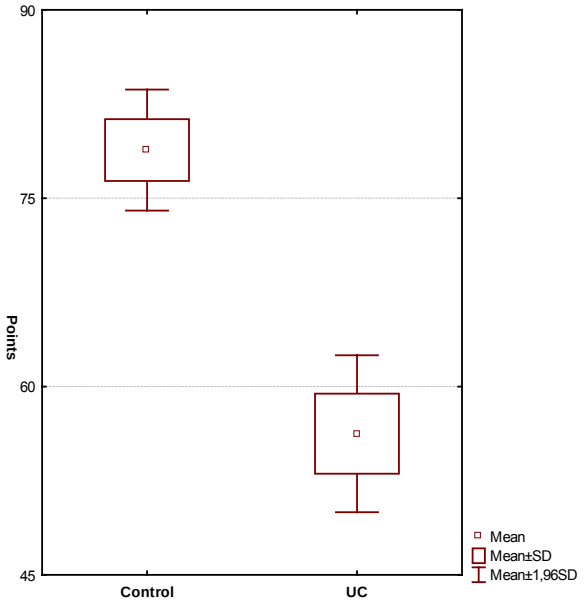

Fig. 4. Bodily Pain-comparison between the control group and UC patients

The UC patients declared pain more often than the control group. Their mean score was 56 points, while for healthy people it was 78 points.

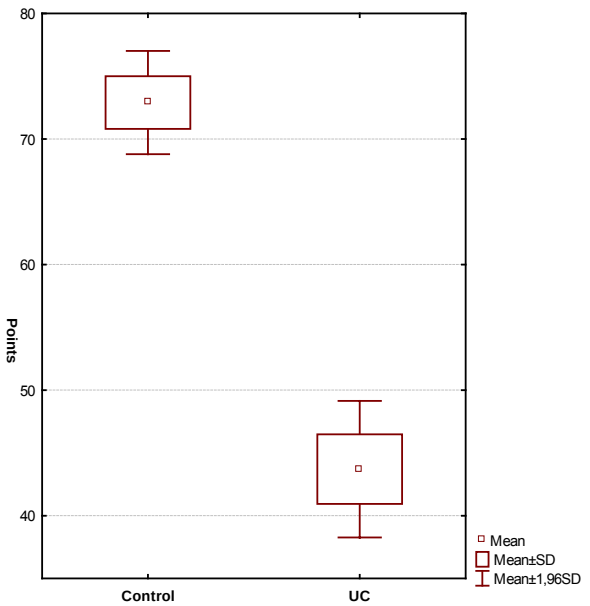

Fig. 5. General Health-comparison between the control group and UC patients

The UC patients estimated their heath to be worse (mean score 44 points) than the control group (mean score 72 points). This difference stemmed from their awareness of chronic and recurrent character of the disease and concerns of exacerbation.

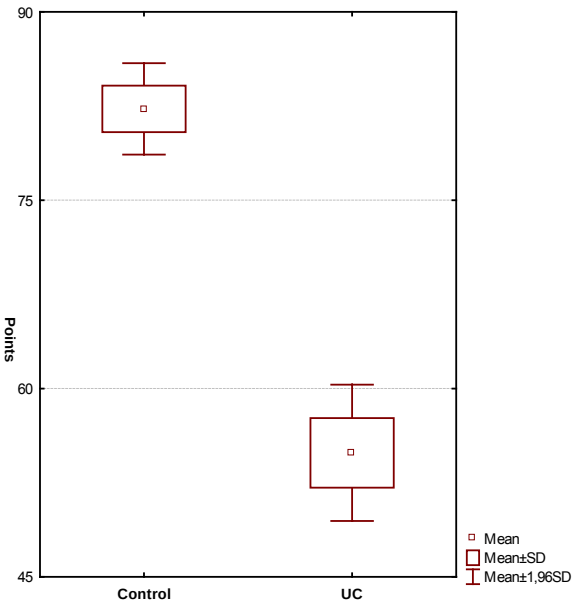

Fig. 6. Physical Summary Component-comparison between the control group and UC patients

The Physical Summary Component was created summing up 4 dimensions mentioned above. It gave a full picture of somatic disturbances and resultant consequences. The UC patients achieved much less score (64 points) than healthy people (83 points) in this category.

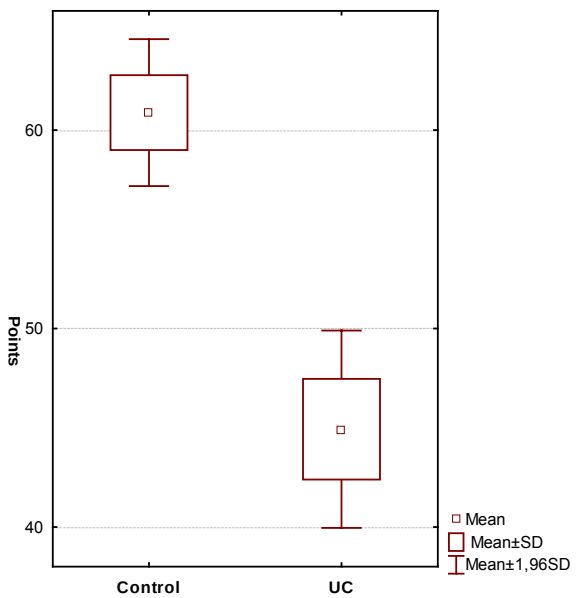

Fig. 7. Vitality-comparison between the control group and UC patients

Vitality in the group of people with UC was scored at 45 points whereas in the control group it was 61 points. One might concluded that the UC patients felt tired much more often and they were seldom cheerful and full of energy.

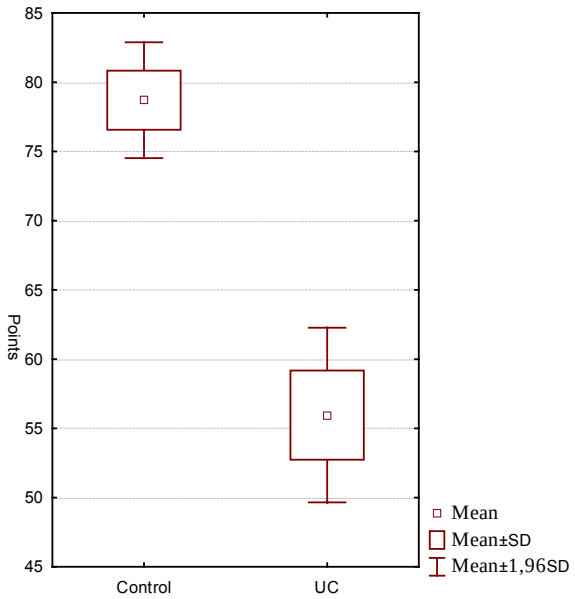

Fig. 8. Social Functioning-comparison between the control group and UC patients

The UC group in respect to Social Functioning represented the mean score of 56 points, whereas the background population 77 points. The CU patients had much more difficulties with social activities such as visiting friends and relatives.

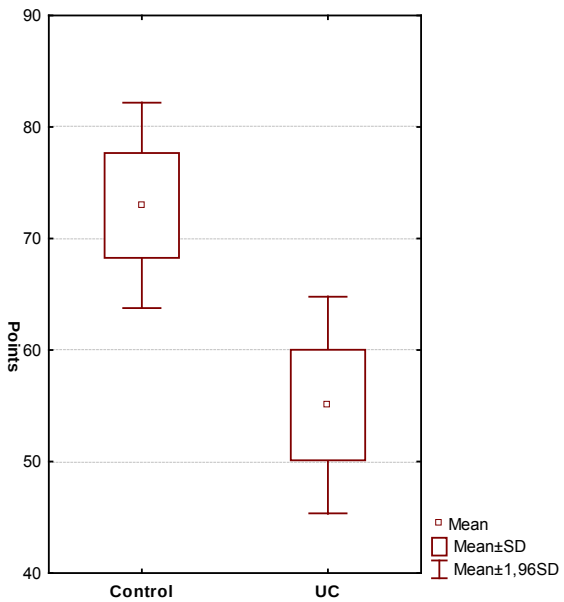

Fig. 9. Role Emotional-comparison between the control group and UC patients

Role Emotional-the UC patients had to limit their working time. As the consequence, they achieved much less than they would like to. This conclusion stemmed from the fact that the sufferers scored 56 points, whereas the healthy-72 points.

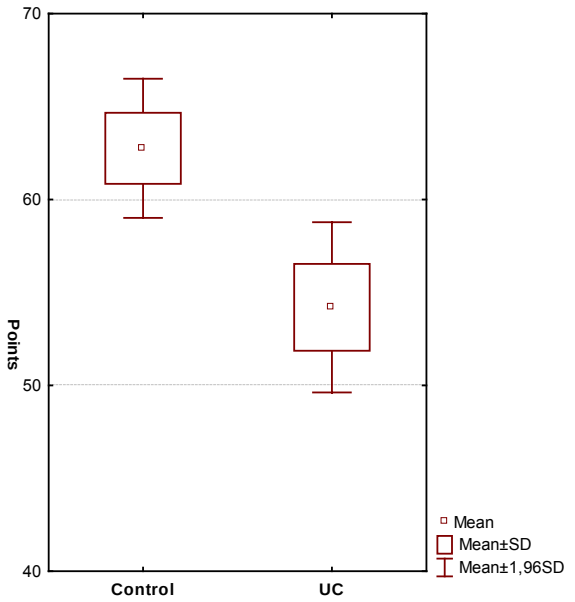

Fig. 10. Mental Health-comparison between the control group and UC patients

Mental Health –the mean score for background population was 62 points whereas for the UC patients 54 points. The UC patients were much more often anxious and easily get upset.

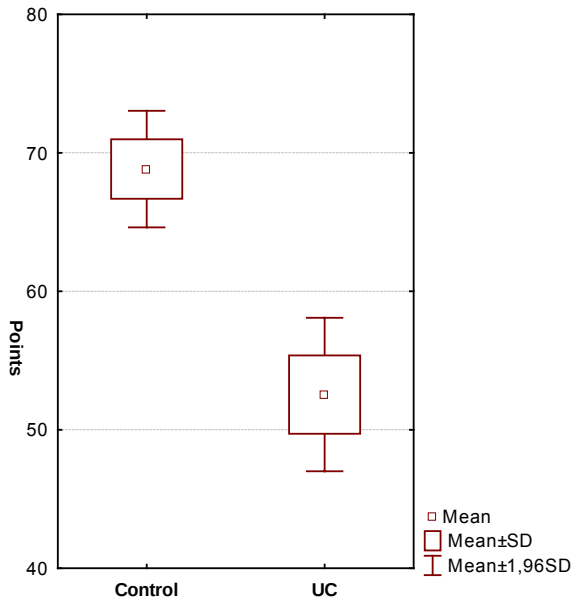

Fig. 11. Mental Summary Component-comparison between the control group and UC patients

Mental Summary Component was created as a summary measure by combining four dimensions mention above. In each individual dimension the UC sufferers scored lower than the control. The collective dimension shows analogical results.

In the study population worse quality of life in elderly patients was observed. It was shown by a negative correlation coefficient. The reason for this phenomenon is that elderly

people had more chronic diseases (different than UC), as well as more specific health and community problems [5].

Discussion

The interest of psychological aspect in the run of IBD has increased recently. Similarly to majority of chronic diseases this group of disorders impacts physical, economical and social aspects of life. Very important is that the fact of being ill has psychological implications.

The present results show that quality of life during remission of ulcerative colitis is decreased [6] as described in the article: "Impairment of health-related quality of life in patients with inflammatory bowel disease…" .Cellas et al. says: CD impairs patients' HRQOL, and the degree of impairment depends on disease activity".

Decreased quality of life has impact on worse physical as well as psychological functioning. The worse psychical functioning could be caused by: extra-intestinal manifestation of IBD (skin, joint lesions), side effects of steroid therapy, symptoms analogical to those occurring in IBS (not specific bowel pains, changes in frequency of defecation, dyspepsia) [7]. Anxiety and depression could have impact on response to standard pharmacological treatment in the case of chronic diseases. Depression and anxiety are common among IBD sufferers, frequency of this disorders is estimated at 30% in comparison to the general population [8].Psychical functioning of people with CU is decreased in comparison to the control group. Contradictory data concerning impact of psychological condition on the course of IBD are presented in literature. Some authors regard psychological background as independent factor responsible for induction of exacerbations [8]. Mittermaier et al says: "Our data indicate that depressive mood associated with anxiety and lower HRQOL may be a risk factor for early clinical recurrence". States of increased stress and anxiety can cause flare-up. On the other hand, awareness of chronic disease, continuous pharmacotherapy and risk of complications could be responsible for secondary character of depressive disorders. In the study group the dependence quality of life from age was proved in the group of study [2].

The source for this phenomenon could be fact that elderly people have more chronic diseases and their social roles have changed [2]. The reason also could be more serious run of IBD in elderly patients. In our group of patient it was failed to prove that there is a difference in the course of CU in women and men, despite such dependence described in literature [9].

Conclusions

Patients with ulcerative colitis shows much worse functioning physical and psychical in comparison to the control group (the healthy).

Elderly patients have much decreased quality of life in the population under consideration.

The treatment of patients with IBD should have interdisciplinary character. Beside internist care, which is aimed on somatic disorders minimization, it is essential to consider psychological (or psychiatric) consultation [10]. The access to regular psychological consultation is needed to decrease anxiety, tension and in consequence to help the patients to profit from life and interpersonal contacts. Such care is important due to psychical aliments which are considered as factors shortening the remission and induct exacerbation.

References

1. A. Szczeklik "Choroby wewnętrzne" p. 816-822, Medycyna Praktyczna, Kraków 2005.
2. A. G. Pallis, I. G. Vlachonikolis, I. A. Mozuas "Assessing health-related quality of life with patients with inflammatory bowel disease, in Crete, Greece" BioMed Cenrtal Gastroenterology 2:1, 2002.
3. F. Casellas, J. López-Vivancos, X. Badia, J. Vilaseca, J. R. Malagelada "Influence of inflammatory bowel disease on different dimensions of quality of life" European Journal of gastroenterology and Hepatology 13(5):567-572, 2001.
4. I. McDowell, C. Newell "Measuring Health", p. 446-454, Oxford University Press 1996.
5. G. A. Akerkar, M. A. Peppercorn "Inflammatory bowel disease in elderly. Practical treatment guidelines" Age & Aging 10:199-208, 1997.
6. F. Casellas, J. I. Arenas, J. S. Baudet, S. Fábregas, N. García, J. Gelabert, C. Medina, I. Ochotorena, M. Papo, L. Rodrigo, J. R. Malagelada "Impairment of health-related quality of life in patients with inflammatory bowel disease: a Spanish multicenter study" Inflammatory Bowel Disease 11(5):488-496, 2005.

Table 3. Assessment of relationship between physical dimension and age of UC sufferers

	value	PF	RP	BP	GH	PCS
Age	r	-0.404	-0.351	-0.224	-0.377	-0.396
	p	p=0.001	P=0.001	p=0.004	p=0.001	p=0.001

Table 4. Assesment of relationship between psychical dimension and age of UC sufferers

	value	V	Scof	ER	MH	MCS
Age	r	-0.214	-0.356	-0.152	-0.240	-0.270
	p	p=0.007	p=0.001	p=0.056	P=0.002	p=0.001

7. M. Simeren, J. Aelsson, R. Gillberg, H. Abrahamsson, J. Svedlund, E. S. Bjornsson "Quality of life in inflammatory bowel disease in remission: the impact of IBS-like symptoms and associated" abstract PubMed, 2002.
8. Ch. Mittermaier, C. Dejaco, T. Waldhoer, A. Oefferlbauer--Ernst, W. Miehsler, M. Beier, W. Tillinger, A. Gangl, G. Moser "Impact of depressive mood on relapse in patients with inflammatory bowel disease: A Prospective 18-month follow-up study" Psychosomatic Medicine, 79-84, 2004.
9. S. Saibeni, I. Cortinovis, L. Beretta, M. Tatarella, L. Ferraris, E. Rondonotti, A. Corbellini, A. Bortoli, E. Colombo, C. Alvisi, G. Imperiali, R. de Franchis "Gender and disease activity influence health-related quality of life in inflammatory bowel disease" Hepatogastroenterology 52(62):509-515, 2005.
10. E. Gómez-Gil, A. Vidal, J. Panés, J. Jaén, J. M. Peri, E. Fernández-Egea, J. M. Piqué "Relationship between patent's subjective stress perception and the course of inflammatory bowel disease" abstract PubMed, 2003.

PHYSICIAN	⟷	**STATISTICIAN**